

1 **A tale of three islands: downstream natural iron**
2 **fertilization in the Southern Ocean**

J. Robinson^{1,2}, E. E. Popova¹, M. A. Srokosz¹, A. Yool¹

3 **Key points:**

4

5 • Iron fertilization of blooms downstream of Southern Ocean islands studied with Lagrangian
6 modelling

7

8 • Ocean areas fertilized by simulated iron transport overlap with observed spatial extent of
9 blooms

10

11 • Inter-annual variability of iron input explains blooms at Crozet but not Kerguelen or South
12 Georgia

13

¹National Oceanography Centre, U.
Southampton Waterfront Campus,
European Way, Southampton, SO14 3ZH,
UK.

²Ocean and Earth Science, U.
Southampton, University Road,
Southampton, SO17 1BJ.

14 **Abstract.** Iron limitation of primary productivity prevails across much
15 of the Southern Ocean but there are exceptions; in particular, the phy-
16 toplankton blooms associated with the Kerguelen Plateau, Crozet Islands
17 and South Georgia. These blooms occur annually, fertilized by iron and
18 nutrient-rich shelf waters that are transported downstream from the is-
19 lands. Here we use a high-resolution ($1/12^\circ$) ocean general circulation
20 model and Lagrangian particle tracking to investigate whether inter-annual
21 variability in the potential lateral advection of iron, could explain the inter-
22 annual variability in the spatial extent of the blooms. Comparison with
23 ocean color data, 1998 to 2007, suggests that iron fertilization via advec-
24 tion can explain the extent of each island's annual bloom, but only the
25 inter-annual variability of the Crozet bloom. The area that could poten-
26 tially be fertilized by iron from Kerguelen was much larger than the bloom,
27 suggesting that there is another primary limiting factor, potentially sili-
28 cate, that controls the inter-annual variability of bloom spatial extent. For
29 South Georgia, there are differences in the year-to-year timing of advection
30 and consequently fertilization, but no clear explanation of the inter-annual
31 variability observed in the bloom's spatial extent has been identified. The
32 model results suggest that the Kerguelen and Crozet blooms are terminated
33 by nutrient exhaustion, probably iron and or silicate, whereas the deepening
34 of the mixed layer in winter terminates the South Georgia bloom. There-
35 fore, iron fertilization via lateral advection alone can explain the annual
36 variability of the Crozet bloom, but not fully that of the Kerguelen and

³⁷ South Georgia blooms.

³⁸

1. Introduction

39 It is now generally accepted that iron, in conjunction with light, is a major limiting
40 factor of primary production in the Southern Ocean, indirectly controlling the biologi-
41 cal pump and drawdown of carbon dioxide from the atmosphere [*Takahashi et al.*, 2009;
42 *Blain et al.*, 2007; *Boyd et al.*, 2007; *de Baar et al.*, 1995; *Martin*, 1990; *Martin et al.*,
43 1990]. However, there are exceptions to the high nutrient, low chlorophyll conditions that
44 prevail across most of the Southern Ocean. Large phytoplankton blooms are observed
45 downstream of continental shelf and land mass [*Blain et al.*, 2007; *Pollard et al.*, 2007;
46 *Korb et al.*, 2008], where iron is suggested to be supplied to surface waters predominately
47 from ocean sediments [*Bakker et al.*, 2007; *Tyrrell et al.*, 2005; *Thomalla et al.*, 2011]. In
48 order to understand these important high productivity regions, we need to characterize
49 the timescales and mechanisms that transport iron to where primary production occurs
50 [*Boyd et al.*, 2012; *d'Ovidio et al.*, 2015; *Wadley et al.*, 2014]. Here we focus on three
51 Southern Ocean islands groups, the Kerguelen Plateau, Crozet Islands and South Georgia
52 and Shag Rocks, outlined by black boxes in Figure 1a, specifically looking at the role of
53 advection in determining the spatial extent of the downstream blooms.

54
55 Iron supply in the Southern Ocean comes from a variety of different sources including:
56 aeolian input; brine rejection and drainage from sea ice; sediments; entrainment from the
57 deep ocean via winter mixing, Ekman pumping, and upwelling at ocean fronts; and it
58 is also constantly resupplied via rapid recycling of organic material [*Boyd and Ellwood*,
59 2010; *Gille et al.*, 2014; *Graham et al.*, 2015; *Korb et al.*, 2008; *Schallenberg et al.*, 2015;

60 *Tagliabue et al.*, 2014]. A recent study by *Graham et al.* [2015] suggests that coastlines,
61 continental and island, are key sources of iron to the Southern Ocean, and also provides a
62 comprehensive description of the behavior of iron in sediment pore waters and the mech-
63 anisms behind its flux into over-lying bottom water. Another source, recently found to
64 be relevant to the Kerguelen Plateau, is riverine input associated with snowmelt. This
65 source is important during spring, as there is increased rainfall and runoff, whereas freez-
66 ing conditions during the winter inhibit this iron supply [*van der Merwe et al.*, 2015]. In
67 this paper we focus on the potential for iron fertilization from island sources, primarily
68 from sediments and run-off.

69
70 As iron is released from island sediments, internal waves and turbulence mix the iron
71 up into surface waters which then fuels phytoplankton production [*Bowie et al.*, 2015;
72 *Boyd*, 2007; *Korb et al.*, 2008; *Park et al.*, 2008]. Iron that is not immediately utilized by
73 biota or scavenged from the water column can be transported downstream of its source
74 via lateral advection within the local circulation and also by stirring within mesoscale fea-
75 tures [*Abraham et al.*, 2000; *d'Ovidio et al.*, 2015]. As it advects, iron can undergo many
76 processes and transformations as part of the complex iron cycle, which can alter both the
77 transport and bioavailability of iron. For instance, iron can be diluted by physical mixing,
78 it can be kept in circulation by iron-binding ligands, or there can be luxury uptake of the
79 iron by biota and hence “internal advection” [*Mongin et al.*, 2008]. In various forms, iron
80 can be lost from the surface by sinking or it can be retained in the surface water and then
81 remineralized downstream of the original source and supply a new area with iron [*Boyd*

82 *et al.*, 2000; *Boyd*, 2007].

83

84 In order to test the hypothesis that inter-annual variability observed in the spatial ex-
85 tent of downstream island blooms could be explained by horizontal advection, the details
86 of the iron cycle are not considered here. In this paper the term "iron advection" refers
87 to any iron from island sources in a form that can be laterally transported, via either ad-
88 vection or stirring, and is also bioavailable at the bloom site, hence what is demonstrated
89 in this paper is the potential for iron fertilization. To diagnose the advection around
90 each island, Lagrangian particles were released within velocity fields from the NEMO
91 (Nucleus for European Modelling of the Ocean) 1/12° ocean general circulation model, a
92 resolution high enough to resolve eddies and small scale circulation patterns around the
93 islands. In the analysis the Lagrangian trajectories, representing water mass potentially
94 fertilized with iron, are compared against the observed bloom areas in the satellite data.
95 Additionally, the possible causes for bloom termination will be considered for each island,
96 utilising the model diagnostics and also World Ocean Atlas nutrient data.

97

2. Methodology

98 In order to assess the impact of iron that could potentially be advected downstream of
99 Southern Ocean islands, satellite derived data (chlorophyll-a concentrations and sea sur-
100 face currents) were compared with Lagrangian particle trajectories within velocity output
101 from the NEMO 1/12° model. Here we give a brief description of each of the three study
102 sites, the tools used, and explain the experimental design.

103

2.1. Study sites

104 The Kerguelen Plateau and Heard Island (southeast of the Kerguelen Island), depicted
105 by the box on the right of Figure 1d (bathymetry plot), is a major bathymetry feature
106 within the Indian Ocean sector of the Southern Ocean, extending from 46°S to 64°S at the
107 3000 m isobath. It forms a major barrier to the eastward flowing Antarctic Circumpolar
108 Current (ACC), with most of the flow being deflected to the north of the plateau (\sim
109 100 Sv), and the substantial remainder to the south (30–40 Sv), steered primarily by the
110 topography. The circulation over the plateau between the two islands is rather stagnant,
111 $<5 \text{ cm}^{-s}$ on average. A major circulation feature within the region is the Polar Front
112 (PF), which cuts between the two islands, flowing close to the southeast Kerguelen Island
113 [Park *et al.*, 2008, 2014]. The Kerguelen bloom occurs on decadal average during Novem-
114 ber to January, as demonstrated in Figure 3a., and is predominately made up of diatom
115 species above the plateau [Blain *et al.*, 2001]. However, note that the Kerguelen bloom
116 can persist for much longer periods, due to a concurrent resupply of essential nutrients via
117 remineralisation and entrainment from the deep ocean during vertical mixing [Boyd, 2007].

118
119 Crozet Islands (46°S, 52°E), depicted by the central black box in Figure 1d, is separated
120 from the Del Cano Rise plateau to the west by the Subantarctic Front (SAF), which is the
121 dominant circulation feature in the area. The SAF predominately lies west to east within
122 the ACC, but turns sharply north between the two plateaus (Crozet and Del Cano Rise),
123 before turning eastward to the north of Crozet as it comes into contact with the Agulhas
124 Return Current [Bakker *et al.*, 2007; Pollard *et al.*, 2007]. Over the plateau and to the
125 north of the island (bounded by the SAF) is an area of Polar Frontal Zone characterised

126 by weak circulation (15 – 20 Sv), within which iron can accumulate during the winter
127 months that can subsequently fuel a bloom [*Planquette et al.*, 2007]. The phytoplankton
128 community structure of the Crozet bloom, described by *Poulton et al.* [2007], is made
129 up of varying sizes of diatoms, and very small prymnesiophyte *Phaeocystis antarctica*.
130 Biomass varies considerably near to the plateau between species, but further away from
131 the plateau, to the northwest and east, prymnesiophyte *P. antarctica* can dominate.

132
133 South Georgia, and Shag Rocks (northwest of South Georgia), hereafter referred to
134 collectively as South Georgia, are located to the east of Drake Passage, highlighted by the
135 left black box in Figure 1d. The islands form part of the North Scotia Ridge at roughly
136 54°S, 37°W, directly in the path of the ACC. The PF lies north of the islands, and the
137 Southern ACC Front flows to the south, looping anti-cyclonically around South Georgia
138 before flowing east again [*Orsi et al.*, 1995; *Meredith et al.*, 2003]. North of the island,
139 enclosed by the PF and Southern ACC Front, is the South Georgia Basin, within which
140 prolonged blooms exist throughout the growing season [*Borrione and Schlitzer*, 2013].
141 This paper will focus on the South Georgia Basin bloom, but there are blooms occurring
142 to the south and west of the islands [*Ward et al.*, 2007], although these blooms are partly
143 subsurface and may not be represented by satellite observations. Furthermore the region is
144 one of the most productive regions across the entire Southern Ocean, with various sources
145 of iron and phytoplankton [*Ardelan et al.*, 2008; *Murphy et al.*, 2013; *Thomalla et al.*,
146 2011]. Consequently, from satellite ocean color data alone, it is not possible to delineate
147 blooms fertilised by iron from South Georgia sediments or from elsewhere within the basin
148 (Antarctic peninsula or ice melt). The South Georgia Basin bloom (hereafter referred to

149 as the South Georgia bloom) is dominated by large diatom species, but is described as
150 “patchy” over scales of 10 – 20 km, with fragmented diatom colonies occurring alongside
151 a more invariant community of small autotrophs and heterotrophs [*Atkinson et al.*, 2008;
152 *Korb et al.*, 2008].

153

154 Each of the three islands have different characteristics which determine the ecosystem
155 that they support and its functioning, but for a generalized overview of the Southern
156 Ocean ecosystem see *Boyd* [2002]. These islands have been selected for this study as their
157 blooms have been extensively explored in the field [*Blain et al.*, 2008; *Pollard et al.*, 2007;
158 *Korb et al.*, 2008; *Murphy et al.*, 2013], the results from which can be used to support our
159 own analysis.

160

2.2. Satellite data

2.2.1. Chlorophyll observations

162 The ocean color data used in this study comes from the ESA Ocean Colour Climate
163 Change Initiative. Here we use a (level 3 geographically mapped) merged and bias cor-
164 rected product from the MERIS, MODIS and SeaWiFS datasets, with a horizontal reso-
165 lution of up to 4 km [*Storm et al.*, 2013]. Because of the low solar elevation and sea-ice
166 coverage in winter, data is unavailable in some areas, most visibly the Weddell Sea in
167 Figure 1a, but by averaging over a month, year and decade, we can fill in many of the
168 gaps. This study has utilized monthly chlorophyll-a (chl-a) concentrations over the pe-
169 riod 1998 – 2007, the first decade in which we have good satellite coverage across the
170 world. In this study, the chlorophyll data is used to represent phytoplankton biomass,

171 defining the island blooms.

172

173 **2.2.2. Altimetric sea surface currents**

174 The satellite altimeter data is produced by Ssalto/Duacs and distributed by the Archiving
175 Validation and Interpretation of Satellite Data in Oceanography (Aviso) group, with
176 support from CNES (<http://www.aviso.altimetry.fr/duacs/>). Here we utilize a
177 merged dataset, from only two satellites at any one time, each having the same ground
178 track and stable sampling which provides a homogenous time series. This along-track,
179 delayed time data product has great stability and therefore is the ideal product for use in
180 inter-annual comparison studies [*Le Bars et al.*, 2014].

181

182 The along-track Absolute Dynamic Topography (ADT) is obtained by adding the
183 Sea Level Anomaly to the Mean Dynamic Topography (Mean Sea Surface Height minus
184 Geoid). A mapping procedure using optimal interpolation with realistic correlation
185 functions is applied to produce ADT maps (MADT or L4 products) onto a Cartesian $1/4^\circ$
186 x $1/4^\circ$ grid [*Aviso*, 2014]. Here we use the sea surface geostrophic velocities computed
187 from the ADT over the period of 1998 – 2007.

188

2.3. NEMO model and Ariane Lagrangian particle tracking

189 The NEMO $1/12^\circ$ resolution ocean general circulation model has been developed with
190 particular emphasis on realistic representation of fine-scale circulation patterns [*Madec*,
191 2008], which provides an ideal platform to conduct Lagrangian particle-tracking exper-
192 iments around the small islands of the Southern Ocean. Full details of the model run,

193 including model setup and configuration, can be found in *Marzocchi et al.* [2015] as only
194 a brief description will be given here. The model is initialized with World Ocean Atlas
195 (WOA) 2005 climatological fields and forced with 6-hourly winds, daily heat fluxes, and
196 monthly precipitation fields [*Brodeau et al.*, 2012]. The run begins in 1978, with output
197 through to 2010, of which we are interested in 1998 – 2007. Model output is stored offline
198 as successive 5 day means throughout the model run, of which the velocity fields are used
199 for the particle tracking in this paper.

200

201 The Ariane package [*Blanke & Raynaud*, 1997] (available online at: <http://stockage.univ-brest.fr/~grima/Ariane>) is applied to the NEMO velocity field to track water
202 parcels using point particles that are released into the modeled ocean circulation (cf.
203 *Popova et al.* [2013] and *Robinson et al.* [2014], who used output from the NEMO 1/4°
204 model). These particles are intended here to represent water masses fertilized by iron
205 scoured from the island sediments. Further details about the Ariane package can be
206 found in *Blanke & Raynaud* [1997] and *Blanke et al.* [1999].

208

209 An important caveat to the results is that we do not expect the NEMO 1/12° model
210 to reproduce the detailed mesoscale flows year-by-year due to chaotic dynamics, as the
211 mesoscale eddy field is not initialised to match that of the real world (only possible using
212 data assimilation). Nevertheless, the model does reproduce the larger scale flow field in the
213 vicinity of the islands, which is important for downstream advection (see Figure 1b and c).

214

2.4. Experiment design

215 In order to study the advection of iron from island sources and make a qualitative
216 comparison with the ocean color 1998 – 2007 observations, Lagrangian particles were re-
217 leased monthly into the modeled circulation from around the shelf regions of each island,
218 from January 1998 to December 2007. Particles are deployed in every other grid cell of
219 the $1/12^\circ$ model grid along the horizontal (latitudinally and longitudinally), and at each
220 level of the NEMO grid depth domain down to a maximum depth of 180 m (30 depth
221 levels, not equally spaced see *Madec* [2008]), around each of the three islands (cf. *Srokosz*
222 *et al.* [2015], who used a similar analysis for the Madagascar bloom). Figure 2 shows the
223 starting positions of the particles around each of the islands. The particles had to be
224 spaced at a high enough resolution to resolve the fine scale circulation patterns around
225 each island, but the experiments were limited computationally, as the islands are not of
226 a comparable area, so there could not be a particle within every model grid cell. The
227 particles are released in both the horizontal and vertical extent, to represent iron that is
228 scoured from the shelf sediment (down to 180 m in this experiment) and mixed upwards
229 [*Ardelan et al.*, 2008; *Blain et al.*, 2001; *Hewes et al.*, 2008; *Planquette et al.*, 2007] as well
230 as other island sources, such as river run-off [*van der Merwe et al.*, 2015]. Particles that
231 are subducted deeper than 200 m, i.e. out of the euphotic zone, along their trajectory are
232 removed from the analysis. At the horizontal and vertical grid spacing described, that
233 results in 8240 Lagrangian particles being released each month from the Kerguelen and
234 Heard Island, 465 particles from Crozet, and 2820 particles from South Georgia and Shag
235 Rocks.

236

237 **2.4.1. Assumptions and limitations of method**

238 The main assumption in this study is that surface waters in the Southern Ocean are iron
239 limited, and that the addition of iron to an area, via horizontal advection, would initiate
240 a bloom. However in reality, productivity can be co-limited in the Southern Ocean, with
241 light or silicate for example, and there are also seasonal factors which control phytoplank-
242 ton growth, which can vary in both time and space [Boyd, 2002].

243
244 In the analysis to follow, the advection time over a period of twelve months is discussed.
245 Note that the residence time of bioavailable iron in surface waters is not yet fully under-
246 stood, but thought to be relatively short, on the order of only weeks to months [Boyd and
247 Ellwood, 2010; Shaked and Lis, 2012; Schallenberg et al., 2015]. However, studies have
248 also shown that iron can be transported during winter months and remain in the upper
249 ocean to be available to stimulate blooms in the summer months [Mongin et al., 2009;
250 d'Ovidio et al., 2015]. Graham et al. [2015] postulates that this might be possible due to
251 intense biological recycling of iron, or the long-range transport of particulate iron, or even
252 by currently unknown processes. For the time being these questions remain unanswered,
253 and so for the purpose of this study all of the iron from the islands is assumed to remain
254 available throughout the year. A further assumption is that all advective pathways have
255 the potential to be fertilized with iron.

256
257 A caveat to this analysis is that, in using satellite ocean color data, it is not possible to
258 detect subsurface chlorophyll maxima, which are known to exist in certain regions of the
259 Southern Ocean [Holm-Hansen et al., 2005; Tripathy et al., 2015]. Therefore we cannot

260 use our analysis to draw any conclusions on the location or variability of known subsurface
261 chlorophyll maxima [*Ward et al.*, 2007], and make the distinction now that only surface
262 blooms are considered, hereafter just referred to as blooms.

263

264 As touched upon in the introduction, the representation of iron and its transport in
265 this method is a simplification. Ideally this study would be performed using tracers in
266 a high-resolution, fully coupled biogeochemical model, but the computational resources
267 required for this would be extreme. Such a study would need a coupled model at a res-
268 olution high enough to formally resolve the small-scale circulation features that occur
269 around the islands at the center of this study. As such, the analysis presented in our re-
270 sults and discussion is restricted to consider only potential iron advection and consequent
271 fertilization.

272

3. Results

3.1. Ocean color

273 Figure 1a is a 10 year average of satellite derived sea surface chl-a concentrations in
274 November, over 1998 to 2007. The islands of interest are highlighted by black boxes,
275 from which it is clear that these island blooms can be more than double the magnitude
276 of productivity anywhere else in the Southern Ocean. Figure 3 is the decadal monthly
277 averages, of surface chl-a concentration, for a single location inside, and a single loca-
278 tion outside of the bloom sites for each island. Each location was selected arbitrarily
279 based on persistence either inside or outside (upstream of the ACC) of the annual bloom.
280 The latitude and longitude coordinates of each location inside the bloom are 72°E and

281 49°S, 52.5°E and 45.5°S, 38.5°W and 52.5°S; for Kerguelen, Crozet and South Georgia
282 respectively. The coordinates of each location upstream of the bloom are 66°E and 48°S,
283 45.5°E and 46.5°S, 49.5°W and 52.5°S (cf. *Park et al.* [2008] their figure 11, *Pollard et al.*
284 [2009] their figure 1, and *Korb et al.* [2004] their figure 1, for schematic positioning of the
285 ACC around Kerguelen, Crozet and South Georgia respectively). In this paper, a bloom
286 is defined by chl-a concentrations higher than 0.5 mg m^{-3} , as it is consistently higher
287 than chl-a outside of each islands typical bloom regions [*Comiso et al.*, 1993; *Moore and*
288 *Abbott*, 2000]. Also, when 0.5 mg m^{-3} of chl-a is exceeded in Figure 3, it occurs on a
289 steep gradient from one month to the next, indicating the start of a bloom. Addition-
290 ally this concentration is low enough to avoid complications with double peaks in chl-a
291 associated with South Georgia, as can be seen in Figure 3c. South Georgia is a region
292 that frequently has two bloom peaks per year [*Borrione and Schlitzer*, 2013], however it
293 is outside of the scope of this work to analyze peak bloom events. Therefore, in order
294 to focus on inter-annual rather than inter-seasonal variability, we consider the average
295 chl-a concentration over the bloom period. The error bars in Figure 3 are 1 standard
296 deviation in chl-a for each month, over the ten year period. The size of the error bars is
297 an indication of the seasonality across the regions and annual cycles. South Georgia in
298 particular, has large error bars which is due to the range in magnitude of annual blooms.
299 For instance, the average chl-a for January over 1998 – 2007 is $<1 \text{ mg m}^{-3}$, however in
300 January of 2002, the concentration was as high as 15 mg m^{-3} [*Korb and Whitehouse*, 2004].

301

302 Figure 3 also includes the averaged (decadal) monthly mixed layer depth (MLD) in the
303 ‘bloom’ site for each island, calculated online in the NEMO model. Comparing the bloom

304 and MLD curves we see that the bloom is likely triggered by the onset of a shallowing
305 mixed layer [Venables and Moore, 2010]. The MLD, specifically its role in terminating
306 the blooms, is considered in further detail in the discussion.

307

308 Figure 4 shows example years of a small and a large averaged bloom period (hereafter
309 referred to as the bloom) for each island, during 1998–2007. Maximum and minimum
310 blooms for Kerguelen occur in 2003 and 2000, Crozet is 2004 and 2001, and South Geor-
311 gia is 2002 and 2006. Strikingly, Figure 4 demonstrates the strong inter–annual variability
312 in both bloom magnitude and area, which may be explainable by studying the potential
313 iron advection from the islands.

314

3.2. NEMO vs. Aviso surface current speed

315 The ability of the chosen model to accurately represent the circulation in the study
316 area is critical to the quality of the results. In order to assess the performance of the
317 NEMO 1/12° model we can compare with satellite derived sea surface currents (Aviso).
318 The Aviso data is the geostrophic component of the velocity, whereas the NEMO model
319 is the absolute velocity, but this should not impact a comparison between the two as they
320 are near equal at the surface. By comparing the decadal averages of NEMO and Aviso,
321 side by side (Fig. 1), we can assess the models performance.

322

323 Figure 1[b] and 1[c] are a comparison of the decadal (1998 – 2007) average ocean surface
324 current speed, from NEMO and Aviso respectively, across the Southern Ocean. Qualita-
325 tively, the model correctly captures the major features, and also their magnitude. Fast

326 flowing currents are stronger in the model than Aviso, and also boundaries of fast flowing
327 currents within the modeled circulation are more defined than in the observations. This
328 may be due to data smoothing caused by the correlation function applied to the Aviso
329 data or due to the model under representing sub-mesoscale features. Figures S1 - S3
330 in the supporting information show the decadal, annual and monthly averaged circula-
331 tion, of both model and satellite derived velocities, for each island for illustrative purposes.

332

3.3. Advection of iron towards the bloom site

333 In this paper we hypothesize that the advection of iron downstream of islands allow
334 blooms to occur in the otherwise high nutrient, low chlorophyll regime of the Southern
335 Ocean. Here we investigate the timescales of fertilization, and the degree to which the
336 circulation can impact inter-annual variability, during the period 1998 – 2007.

337

338 The Kerguelen bloom occurs on decadal average during November to January, as demon-
339 strated in Figure 3a. For this analysis, we focus on the average surface chl-a concentration
340 over the bloom period (November to January in Kerguelen’s case) for each year, referred
341 to as the bloom. Figure 5 shows the patch around Kerguelen that could potentially be
342 fertilized with iron by the local circulation in the NEMO model. The fertilized patch
343 is depicted by colored markers, which represent the location of trajectories in October
344 for each year, with the different colors indicating the month in which the particles were
345 released from the island. Strikingly, the fertilized patch is much larger than the bloom
346 extent, represented by black contours in each annual subplot. The trajectories propagate
347 east from the island between the latitude band of roughly $45^{\circ}\text{S} - 54^{\circ}\text{S}$, but then spread

348 both northward and southward in extent from roughly 77°E . However, despite the fertil-
349 ized patch reaching as far north as 40°S in Figure 5, we can see from the black contours
350 that the bloom area is never north of 45°S in any of the years.

351

352 Having found that the horizontal advection of iron would be sufficient to fertilize the
353 bloom in principle, a further question arises as to whether the bloom is terminated by the
354 exhaustion of iron in the surface water. This question cannot be addressed directly using
355 the NEMO $1/12^{\circ}$ simulation, as it is not a coupled biogeochemistry model. However, if
356 the bloom is terminated by the exhaustion of iron then a question that can be addressed
357 is: can advection resupply iron in the period between the end of one bloom and the start
358 of the next? As addressed by *Mongin et al.* [2009], and more recently by *d'Ovidio et al.*
359 [2015]. For Kerguelen, the location of the fertilized patch was very consistent, however
360 there are temporal differences in the timing of advection. Nevertheless, the results show
361 the maximum advection time for the particles to reach the furthest extents of the bloom is
362 on the order of 5 – 6 months, suggesting that horizontal advection is sufficient to resupply
363 the bloom area with iron, in agreement with *Mongin et al.* [2009] and *d'Ovidio et al.* [2015].

364

365 Figure 6, is the same as 5, but focusing on Crozet. The Crozet bloom occurs one month
366 earlier than the Kerguelen bloom, on decadal average during October to December [*Pol-*
367 *lard et al., 2007*], and so the trajectories shown in Figure 6 represent the fertilized patch
368 in September. Figure 6 suggests there is more inter-annual variability in the circulation
369 around Crozet than Kerguelen, both spatially and temporally. In Figure 6, the fertilized
370 patch tends to be north of the island and to the east, made up of particles released in

371 June through to August (light green to orange on the color bar). This indicates that the
372 timescale for fertilization, of water mass being within the immediate vicinity of Crozet
373 (where the particles are released) to outside of the bloom area (the black contours), is
374 on the order of 3 – 4 months, however Figure 6 clearly shows the inter-annual variability
375 in this timescale. There are some years in Figure 6 where we see the fertilized patch
376 extending to the west of the island, most visibly in the years 2000, 2002, 2003, and 2007.
377 The color of the markers seen to the west of the island in some of the years show the
378 particles were released earlier in the year, ranging from January (2000) to April (2002).
379 Focusing on the black contours in Figure 6, representing chl-a concentrations above 0.5
380 mg m^{-3} during the bloom period, there are years in which the bloom is propagated to the
381 west also, most clearly apparent in 2000 and 2007.

382

383 The bloom associated with South Georgia occurs on decadal average, during October to
384 April, however South Georgia experiences the highest seasonality of all the three islands
385 in this study. Here we discuss the South Georgia bloom, although the surrounding area is
386 one of the most productive regions within the Southern Ocean [Ardelan *et al.*, 2008; Young
387 *et al.*, 2014], so separating a bloom associated with iron only advected from South Georgia
388 is not non-trivial. In order to address this issue, we have applied a mask to the ocean color
389 data, to remove chl-a that was most likely fertilized from other iron sources in the region,
390 guided by the surface chl-a climatology around South Georgia produced by *Borrione and*
391 *Schlitzer* [2013]. Figure 7 is again, the same as Figures 5 and 6, with the colored markers
392 representing the particle locations in September (preceding the start of the bloom). The
393 extent of the fertilized patch around South Georgia changes annually, although to a lesser

394 degree than around Crozet. What does remain almost annually consistent, is the north
395 and eastward advection of the particles (with the exception of 2006) and an associated
396 bloom occurring within the Georgia Basin, which is just north of the island. In some of
397 the years, most distinctly in 2004 and 2005, there is a well defined boundary edge to the
398 trajectories on the western side of the fertilized patch. This sloping western boundary
399 edge is also apparent in the average bloom area in almost all years (2006 being the most
400 apparent exception). The trajectories and bloom are restricted to the east of this bound-
401 ary due to the eastward flowing PF which acts as a physical barrier [Moore *et al.*, 1999;
402 Korb and Whitehouse, 2004]. The colored markers represent the particles locations in the
403 month of September, and therefore particles that are released at the beginning of Septem-
404 ber have only had one month to be advected, and consequently are the closest to South
405 Georgia. Focusing just on the recently released particles, from August and September
406 (orange and red), it is apparent that, for the majority of the years, this western boundary
407 of both the fertilized patch and bloom area is an important route for iron to be advected
408 away from South Georgia, flowing towards Shag Rocks and then along the PF. This cir-
409 culation feature was also found by Young *et al.* [2011] in their higher resolution regional
410 model, described as a unidirectional link between the two land masses (see their Figure 7).

411

412 Table 1 provides the size of both the annual blooms and fertilized patches around Ker-
413 guelen. As can also be seen in Figure 5, the fertilized patch is much larger than the
414 bloom, and there is more variability in the bloom size than in the fertilized patch. Con-
415 sequently, the annual percentage of the bloom area that is within the fertilized patch is
416 consistently very high, with an average of 77% (st dev ± 6.5). As the fertilized patch is

417 much larger than the bloom area, it would suggest that iron availability is not the only, or
418 at least most important, factor controlling the Kerguelen bloom extent and inter-annual
419 variability. The year 2003 had the largest bloom in our study period, in which the bloom
420 did extend out across and to the southern edges of the fertilized patch. It is possible,
421 that in 2003 the primary limiting factor to the Kerguelen bloom was alleviated so the
422 bloom could extend further out into the regions of available iron. This hypothesis will be
423 considered later in the study.

424
425 Looking at Table 2, the Crozet bloom is a third of the size of the Kerguelen bloom,
426 with an average bloom size of 242,416 km² compared to the Kerguelen average of 782,455
427 km². Focusing on the percentage of the bloom site overlapped by the trajectories (*Fer-*
428 *tilized patch*) for each year, there is a range of 60% – 32% overlap. This is reflected in
429 the percentage of the fertilized patch overlapped by the bloom, ranging from 67% – 34%.
430 Both the bloom area and fertilized patch around Crozet vary annually, and Crozet has
431 the lowest overlap out of the three islands studied.

432
433 The average size of the South Georgia bloom over 1998 – 2007 was 618,645 km², smaller
434 than the average size of the fertilized patch at 742,038 km². In Table 3, we can see a large
435 range in the bloom area around South Georgia across the years, the maximum being
436 946,833 km² in 2002 and the minimum being 414,108 km² in 2006 (see Figure 4). There is
437 also a range in the size of the fertilized patch, although not as large as the range in bloom
438 size. Focusing on the amount of overlap between the bloom and trajectories, we see that
439 the annual bloom overlaps are generally larger than the fertilized patch overlaps (2002

440 and 2003 being the exceptions). This is due to the fertilized patch being larger than the
441 bloom area for the majority of the years. However, as with the other two islands, there is
442 a range in the annual overlaps, which can be explained by a combination of inter-annual
443 variability in the sizes and locations of the annual blooms, and also, to differing degrees for
444 each island, the inter-annual variability in the size and locations of the fertilized patches
445 (Kerguelen being the most consistent, and Crozet exhibiting the most variation).

446
447 Figure 8 shows the overlap of the bloom (bloom period average, chl-a concentration
448 greater than 0.5 mg m^{-3}) by the fertilized patch from each individual monthly release of
449 particles. In the Kerguelen plot, we see a maximum range of around 10 – 25% between
450 years, in the overlap between monthly releases of particles and the average bloom. The
451 cause of this range is a combination of inter-annual variability in both the advection and
452 bloom extent. In comparison with Figure 5 and Table 1, it is apparent that the high-
453 est degree of variability comes from the bloom, although the inter-seasonal variation in
454 advection timing and consequently fertilization could also impact bloom development.
455 Particles released in October, just prior to the start of the bloom, cover around 10 – 15%
456 of the bloom area, with the maximum bloom coverage from releases in April – June for
457 the majority of the years. This gives an advective fertilization timescale of between 5 – 7
458 months for maximum bloom coverage. The circulation on the Kerguelen Plateau itself is
459 known to be sluggish, certain parts even described as stagnant [*Park et al.*, 2014]. This
460 localized slow moving water on the plateau (where particles start) may account for the
461 low bloom overlap percentage by particles released just prior to the start of the bloom

462 (November).

463

464 In Figure 8, Crozet shows less inter-annual variability than Kerguelen, of less than 10%
465 difference between years. The most apparent difference between Crozet, and the other
466 two islands, is that the advective fertilization timescale is much shorter, with maximum
467 bloom overlap from particles released in June – August, which is 2 – 4 months prior to the
468 start of the bloom (typically October). However, Crozet has the lowest bloom overlap,
469 with a maximum of 25% from an August release in 2000. For the majority of the years,
470 the maximum percent coverage of the bloom is below 20%.

471

472 The South Georgia plot of Figure 8 shows a degree of consistency in the timing of fer-
473 tilization, but high variability in the bloom overlap from each monthly release, across the
474 years. The variability in bloom overlap is on the order of 10 – 15%, and the advective
475 fertilization timescale is roughly April – June, 4 – 6 months prior to the typical start of
476 the bloom. The maximum percentage bloom overlap is 40%.

477

4. Discussion

478 Here we consider other factors that could impact the bloom, light limitation and nutri-
479 ent control, before addressing our three main research questions: Can advection explain
480 the extent of the bloom area? Can advection explain the bloom inter-annual variability?
481 And what factors could cause bloom termination?

482

4.1. Light limitation

483 In addition to iron limitation in the Southern Ocean, light limitation also plays an im-
484 portant role in controlling productivity *Wadley et al.* [2014]. The light levels encountered
485 by phytoplankton cells is partly determined by the mixed layer depth (MLD), as they are
486 vertically mixed between high surface irradiance and low subsurface irradiance (*Venables*
487 *and Moore* [2010] – explanations and references therein). To assess the light availability
488 around the islands during the typical bloom periods, Figure 9 shows the decadal average
489 monthly depths of the mixed layer, calculated online in the NEMO model, over 1998 –
490 2007.

491
492 The top row of Figure 9, shows the MLD around Kerguelen which remains in a similar
493 spatial pattern during the bloom period, with a distinct divide between the shallower
494 north and deeper south. During the period 1998 – 2007, the Kerguelen bloom is con-
495 strained to the south of this divide where the MLD is deepest. The middle row shows
496 the MLD around Crozet which exhibits the typical shallowing north to south of the MLD
497 from winter into summer. In Figure 9 the bottom row is a two month decadal average of
498 the mixed layer for the South Georgia region. Two months have been averaged together
499 in order to capture the entire bloom period within the plot, from which we can see the
500 typical north to south shallowing of the mixed layer from winter into summer. Both the
501 Kerguelen and Crozet Islands blooms have typically terminated when the mixed layer is
502 shallow enough for there still to be light available, which suggests that neither bloom is
503 terminated by light limitation [*Venables et al.*, 2007; *Venables and Moore*, 2010]. The
504 South Georgia bloom, however, persists for the entire season and typically ends when the

505 mixed layer begins to deepen in winter, strongly indicating that the bloom is terminated
506 by diminishing light, and not by the exhaustion of iron.

507

4.2. Nutrient control

508 The depth of the mixed layer is also significant for the amount of nutrients being brought
509 to the surface from the deep, such as nitrate and silicate as well as iron. WOA clima-
510 tologies show the concentration of nitrate to be high across much of the Southern Ocean,
511 south of the Sub-Antarctic Front, whereas silicate concentrations decrease rapidly north
512 of the Polar Front [*Boyer et al.*, 2013]. At Kerguelen, during the recent KEOPS 2 cruise
513 (October – November 2011) *Lasbleiz et al.* [2014] found higher concentrations of silicate
514 south of the PF at roughly 72°E, close to the plateau.

515

516 One possible hypothesis is that silicate is the primary limiting factor controlling the
517 large and highly variable Kerguelen offshore bloom (i.e. longitudinally far away from the
518 plateau), both in spatial extent and inter-annual variability. This could explain why the
519 bloom is contained to the south (bloom northern limit of 44°S), where a deeper MLD can
520 mix silicate to the surface, despite the iron potentially being advected and available as far
521 north as 40°S (see Figure 5). Many previous Southern Ocean iron fertilization studies,
522 both artificial and natural, have reported the development of a large diatom bloom in
523 the fertilized patch [*Blain et al.*, 2001; *de Baar et al.*, 2008; *Mongin et al.*, 2008] and
524 consequently, in the region of Kerguelen, depletion of silicate over the plateau [*Mosseri*
525 *et al.*, 2008]. The absence of a non-diatom bloom is explained by the efficient grazing of
526 microbial communities by copepods and salps as suggested by *Banse* [1996] and *Smetacek*

527 *et al.* [2004]. However, the majority of studies have been focused on the bloom above
528 the plateau rather than further downstream, whereas the 2011 KEOPS II cruise focused
529 mainly on the bloom located just northeast of the Kerguelen Islands above the abyssal
530 plain. Their results suggest that the majority of diatom silica production during the bloom
531 event is sustained by ‘new’ silica, supplied primarily from pre-bloom winter water and also
532 vertical supply. As the bloom progresses, the silicon pump is strengthened by the sinking
533 of biogenic silica, and consequently the standing stock of available silica diminishes over
534 time. Estimates for the duration of the high productivity bloom period is on the order
535 of 85-86 days, after which the bloom declines [*Mongin et al.*, 2008; *Closset et al.*, 2014].
536 These conditions could also be true of the far offshore bloom, which in some years extends
537 further east than 95°S (2003, in Figure 5), but further in-situ observations, of both silicate
538 concentrations and bloom composition, would be necessary to either prove or disprove this.

539

4.3. Can advection explain the extent of the bloom area?

540 Focussing now on the circulation around each island, we discuss if the modeled advection
541 can explain the spatial extent of the island blooms. Our results suggest that iron advected
542 from the Kerguelen and Heard Islands could fertilize an area which overlaps the annual
543 bloom extent, but is actually much larger than the area of the bloom. Figure 10 shows
544 that the bloom which occurs over the plateau (southeast of the Kerguelen island) is
545 predominately fertilized by iron advected from Heard island [*Zhang et al.*, 2008]. This
546 is in agreement with a water mass path way study on the plateau using radium isotopes
547 during the 2005 KEOPS cruise, which also found the water mass on the plateau to have
548 originated from Heard island [*van Beek et al.*, 2008].

549 We find that the larger bloom event, which extends as far as 100°E in some years, is
550 mostly fertilized by iron advected from Kerguelen island (see Figure 10), in agreement
551 with *Mongin et al.* [2009] who also performed a modeled advection study on the Kerguelen
552 bloom.

553 During the recent KEOPS II cruise, iron budgets were calculated focusing on blooms
554 occurring on the plateau, and also offshore in the “plume”, which show the importance
555 of a horizontal supply of iron particularly, for the offshore bloom [*Bowie et al.*, 2015].
556 This separation, in the fertilization of the plateau bloom and offshore bloom, is due to
557 the PF which occurs between the two islands, and flows close to the southern and eastern
558 edge of Kerguelen. Using the definition described in *Park et al.* [2014], the thick black
559 contour in Figure 10 represents the modeled location of the PF for the year 2003. The
560 general position and shape of the PF is fairly consistent each year, however the modeled
561 PF does exhibit small annual variations. In Figure 10, it is apparent that the extent of
562 the Kerguelen island trajectories, and also in 2003 the bloom, is strongly bounded (in the
563 south) by the location of the PF.

564
565 The location of the Crozet bloom was different annually, in some years propagating
566 north west, but most frequently to the north east of the island. The fertilized patch is
567 also predominately to the north east of Crozet, but there are exceptions in some years
568 when small narrow currents flow north west from the island. Meridionally, both the fer-
569 tilized patch and consequently bloom area occur northwards of the islands, due to the
570 formation of a Taylor Column around the island vicinity [*Popova et al.*, 2007]. Zonally,
571 the majority of particles are advected by water which has detrained from a branch of the

572 SubAntarctic Front (SAF), and are advected eastward which corresponds with the orange
573 Argo float trajectories in Figure 5 of *Pollard et al.* [2007]. Lagrangian particles which are
574 advected westward are entrained into a secondary branch from the main SAF, which flows
575 anticyclonic around Del Cano Rise (blue drifter trajectories in Figure 5 [*Pollard et al.*,
576 2007]), before eventually turning eastward at roughly 44deg. In Figure 6, we see that
577 the years in which the fertilized patch is propagated to the west (2000, 2002, 2003 and
578 2007), the particle trajectories are from releases earlier in the year, roughly from January
579 to April. This is due to the water mass north of the island (but south of the SAF) being
580 very sluggish, resulting in particle entrainment into the anticyclonic component of the
581 SAF around Del Cano Rise, taking several months.

582

583 The model does show potential iron advection extending into all regions of the Crozet
584 annual bloom areas, however the fertilized patch in the north west was never as large as
585 the blooms which occurred in the north west. *Read et al.* [2007] found that sub-mesoscale
586 features were important in the development and duration of the Crozet bloom, and ac-
587 counted for the bloom's "patchiness". Though the physical model used in this study
588 is at a very high resolution ($1/12^\circ$), it cannot reproduce the exact eddy field behavior
589 year-on-year, and therefore we do not expect the annual bloom to match the annual
590 fertilized patch. Considering the stochastic nature of eddies, we believe the model to
591 have demonstrated that the local Crozet advection is sufficient to disperse iron into all
592 annual extents of the bloom. Furthermore, the NEMO modeled Lagrangian pathways are
593 in general agreement with drifter data and also altimetry-based Lagrangian model results

594 [*Pollard et al.*, 2007; *Sanial et al.*, 2014].

595

596 A bloom associated specifically with iron advected from South Georgia is impossible to
597 delineate in this study, as the surrounding region is one of the most productive areas of
598 the Southern Ocean (Figure. 1a), due to various other sources of iron e.g. the Antarctic
599 Peninsula [*Ardelan et al.*, 2008; *Murphy et al.*, 2013]. Advection from South Georgia is
600 predominately northwards and then eastwards, joining with the ACC, overlapping with
601 the annual blooms that occur in the north easterly region of South Georgia [*Korb et al.*,
602 2004]. There is a striking sloped western edge to both the bloom area and fertilized patch
603 in most years, caused by the position of the PF, which is bounded by the local topography
604 [*Moore et al.*, 1999]. Between South Georgia and the PF and ACC, the modeled advection
605 was annually consistent and likely to fertilize the annually occurring bloom in this area.

606

4.4. Can advection explain the bloom inter-annual variability?

607 The area that could potentially be fertilized with iron via advection around Kerguelen
608 annually extends into a fairly consistent spatial coverage, although there are significant
609 inter-seasonal variations. Despite this, the fertilized patch was much larger than the
610 bloom area in all years of the study period, suggesting that advection alone cannot ex-
611 plain the blooms inter-annual variability. Focussing on 2003, in Figure 10, we see the
612 open ocean bloom extending as far south as 60°S between a southward and then north-
613 ward deviation of the PF (creating a v-shape). However in most years, the bloom area
614 does not closely match the fertilized patch, and in no years does the bloom propagate
615 as far north (bloom northern limit of 44°S) as the Lagrangian particles. Assuming that

616 the modeled spread of Lagrangian particles is correct, this would suggest that another
617 factor is limiting the spread of the bloom into all areas of available iron, a factor which
618 could be the predominate driver of the inter-annual variability. This would support the
619 theory of silicate limiting the Kerguelen bloom, but without more silicate concentration
620 observations in the far offshore area we can only speculate.

621

622 The Crozet blooms during 1998 – 2007 show a high degree of inter-annual variability,
623 most frequently extending far to the east, but in some years to the west and on occasion
624 extending further north than typical. Our results find a similar degree of inter-annual
625 variability in the modeled local circulation around Crozet, both in the timing of fertil-
626 ization (i.e. the speed of advection) and the extent of the fertilized patch (i.e. size and
627 direction of patch). Although the fertilized patch in our model does not closely match the
628 observed blooms, our results do suggest that iron advection could predominately control
629 the inter-annual variability seen in the Crozet bloom.

630

631 The advection of iron from South Georgia annually covers a similar region (a predom-
632 inately north, then eastward flow), although there are exceptions. The timescale for
633 fertilization is highly variable (distance travelled from the iron source out into the bloom
634 area per month), which could have an impact on the bloom.

635

4.5. Factors controlling bloom termination

636 As the NEMO model offers a range of diagnostics, we can also propose possible bloom
637 termination mechanisms for each island. In the modeled MLD data, the region surround-

638 ing Kerguelen does not clearly follow the north to south shallowing of the MLD in summer
639 typical of the Southern Ocean (Figure 9a). There is a very clear divide in the depths of
640 the mixed layer between the shallower north and deeper south at roughly $45^{\circ}\text{S} - 50^{\circ}\text{S}$.
641 The Kerguelen bloom is always to the south of 45°S , however in the WOA dataset there is
642 nitrate available north of this, as well as iron according to our advection results (Figure.
643 5). Additionally, the WOA nitrate concentration is still high in February, so it is unlikely
644 to be nitrate exhaustion that terminates the bloom. We conjecture that as the bloom is
645 constrained to regions with a deep mixed layer, it is dependant on a deep supply of silicate
646 as suggested by *Mongin et al.* [2008], and found to be the case by *Closset et al.* [2014]
647 in the bloom just offshore of the plateau. There is partial evidence from the WOA that
648 the surface silicate concentration downstream of Kerguelen is lower in February, than in
649 the previous three months, however this is based upon very few data. Looking at data
650 from the first KEOPS cruise, figure 1 in the supplementary material of *Blain et al.* [2007]
651 shows the concentrations of both nitrate and silicate from locations inside and outside of
652 the bloom. It shows that inside the bloom there is no silicate but there is nitrate, whereas
653 outside the bloom there is plenty of both, suggesting silicate to be the limiting nutrient.
654 This suggests that the sampling conducted during the KEOPS II expedition close to the
655 plateau [*Closset et al.*, 2014], needs to be repeated further downstream in future field work
656 in order to determine whether the offshore bloom has similar dynamics longitudinally.

657

658 The modeled monthly MLD around the Crozet region does exhibit some inter-annual
659 variability, but typically, shallows north to south from winter into summer, and is shal-
660 lower than 50 m by the end of the Crozet bloom. However the WOA climatology suggests

661 there is still nitrate available in January, which suggests that iron exhaustion most likely
662 terminates the bloom. This is supported by an experiment performed on the CROZEX
663 cruise, where the addition of iron to an area of bloom decline resulted in the stimulation
664 of further phytoplankton growth [*Moore et al.*, 2007].

665

666 The South Georgia bloom is the most variable in this study, varying in both timing
667 and extent. The decadal average bloom period is from October to April, although it can
668 last longer and also start earlier in some years. The nitrate concentration remains high
669 throughout the bloom period, which suggests a deepening mixed layer being the limiting
670 factor for the otherwise persistent South Georgia bloom. This is supported by *Korb et al.*
671 [2008], who found evidence of a persistent supply of both macronutrients and iron, by
672 physical processes, to the area throughout the growing season.

673

5. Conclusions

674 In the high nutrient, low chlorophyll Southern Ocean [*Martin et al.*, 1990; *de Baar et*
675 *al.*, 1995; *Boyd et al.*, 2007], blooms are observed in satellite ocean color data occurring
676 annually downstream of Kerguelen, Crozet and the South Georgia islands. It is generally
677 accepted that the iron limitation prevailing across the Southern Ocean is locally overcome
678 by the horizontal advection of iron from island sources [*Blain et al.*, 2001; *Murphy et al.*,
679 2013; *Sanial et al.*, 2014]. In this study, Lagrangian particle tracking, with the NEMO
680 1/12° ocean general circulation model, was used to assess whether potential iron advec-
681 tion can explain the extent of the blooms, and also their inter-annual variability over
682 the period 1998 – 2007. We also use the modeled circulation and diagnostic variables to

683 consider possible causes of bloom termination for each of the islands.

684

685 We find that lateral advection downstream of the Southern Ocean islands is sufficient
686 to fertilize all areas where annual blooms can occur. The patch fertilized by iron-rich
687 water from Kerguelen is much larger in extent than the area of the bloom, whereas the
688 patch fertilized around Crozet is comparable in size, taking into account inter-annual
689 variability, to the size of the bloom. The patch of water fertilized by iron-rich South
690 Georgia sediments also closely matches with the annual bloom, however delineating a
691 bloom associated only with South Georgia proved problematic.

692

693 The advection around Kerguelen was consistent in spatial extent annually, however the
694 timing of potential fertilization varied inter-seasonally across the years. This could con-
695 tribute to the blooms inter-annual variability, however the results suggest that the far
696 offshore Kerguelen bloom (in some years occurring as far east as 100°E), has another
697 primary factor controlling its inter-annual variability, and we offer the hypothesis of sil-
698 icate being the ultimate limiting factor on a diatom dominated Kerguelen bloom. This
699 hypothesis could be tested with in-situ nutrient sampling of the area, similar to the recent
700 KEOPS II expedition [*Closset et al.*, 2014], or alternatively by a high-resolution coupled
701 biogeochemical model to properly resolve the key biogeochemical and physical processes.
702 The results suggest that the inter-annual variability seen in the Crozet bloom can be
703 explained by variations in the advected iron supply. The fertilized patch around South
704 Georgia was fairly consistent spatially, however it did have variations in the timing of
705 advection from the island out to the bloom site. This potentially could account for the

706 inter-annual variability seen in the South Georgia bloom.

707

708 In assessing the possible causes of bloom termination, we find that nutrient exhaustion
709 is most likely to cause the Kerguelen and Crozet blooms to collapse (silica and iron, re-
710 spectively). Whereas winter convection causing the mixed layer to deepen is most likely
711 the terminating factor of the South Georgia bloom, as physical processes maintain a con-
712 tinual supply of macronutrients and iron to the area, these are unlikely to be limiting
713 [*Korb et al.*, 2008]. Typically, both the Kerguelen and Crozet blooms end well before the
714 mixed layer begins to deepen in winter, whereas the South Georgia bloom persists for the
715 entire season until the mixed layer deepens.

716

717 **Acknowledgments.** The velocity altimeter products were produced by Ssalto/Duacs
718 and distributed by Aviso, with support from CNES ([http://www.aviso.oceanobs.com/](http://www.aviso.oceanobs.com/duacs/)
719 [duacs/](http://www.aviso.oceanobs.com/duacs/)). Ocean Colour Climate Change Initiative dataset, Version 2.0, European Space
720 Agency, available online at <http://www.esa-oceancolour-cci.org/>. This study was
721 carried out using the computational tool Ariane, developed by B. Blanke and N. Grima.
722 The 1/12°S NEMO simulation used in this work was produced using the ARCHER UK
723 National Supercomputing Service (<http://www.archer.ac.uk>). This work was funded
724 by the UK Natural Environment Research Council through a PhD studentship for J.R.
725 (NE/K500938/1), and national capability funding for E.E.P., M.A.S. and A.Y. The data
726 presented in this study can be obtained by contacting the lead author. The authors would
727 like to thank Phillip Boyd and Eugene Murphy, for their feedback which greatly improved

728 the work.

729

References

730 Abraham, E. R., C. S. Law, P. W. Boyd, S. J. Lavender, M. T. Maldonado, and A.
731 R. Bowie (2000), Importance of stirring in the development of an iron-fertilized
732 phytoplankton bloom, *Nature*, 407 (6805), 727-730, doi:10.1038/35037555.

733

734 Ardelan, M. V., O. Holm-Hansen, C. D. Hewes, C. S. Reiss, N. S. Silva, H. Dulaiova,
735 E. Steinnes, and E. Sakshaug (2010), Natural iron enrichment around the Antarctic
736 Peninsula in the Southern Ocean, *Biogeosciences*, 7 (1), 11–25.

737

738 Atkinson, A., M. J. Whitehouse, J. Priddle, G. C. Cripps, P. Ward, and M. A. Brandon
739 (2001), The pelagic ecosystem of South Georgia, Antarctica, *Marine Ecology Progress
740 Series*, 216, 279 - 308.

741

742 Aviso (2014) SSALTO/DUACS User Handbook: (M)SLA and (M)ADT Near-
743 Real Time and Delayed Time Products, CLS-DOS-NT-06-034, SALP-
744 MU-P-EA-21065-CLS, CNES, Ramonville St. Agne, France, ,59pp, ([http:
745 //www.aviso.altimetry.fr/fileadmin/documents/data/tools/hdbk_duacs.pdf](http://www.aviso.altimetry.fr/fileadmin/documents/data/tools/hdbk_duacs.pdf)).

746

747 Bakker, D. C., M. C. Nielsdottir, P. J. Morris, H. J. Venables, and A. J. Watson (2007),
748 The island mass effect and biological carbon uptake for the subantarctic Crozet

- 749 Archipelago, *Deep Sea Research II*, 54, 2174 – 2190, doi:10.1016/j.dsr2.2007.06.009.
- 750
- 751 Banse, K. (1996), Low seasonality of low concentrations of surface chlorophyll in
752 the Subantarctic water ring: underwater irradiance, iron, or grazing?, *Progress in*
753 *Oceanography*, 37 (3-4), 241-291.
- 754
- 755 Blain, S., et al. (2001), A biogeochemical study of the island mass effect in the context
756 of the iron hypothesis: Kerguelen Islands, Southern Ocean, *Deep-Sea Research Part I-*
757 *Oceanographic Research Papers*, 48 (1), 163–187, doi:10.1016/S0967–0637(00)00047–9.
- 758
- 759 Blain, S., et al. (2007), Effect of natural iron fertilization on carbon sequestration in the
760 Southern Ocean, *Nature*, 446 (7139), 1070–1074, doi:10.1038/nature05700.
- 761
- 762 Blain, S., B. Quguiner, and T. Trull (2008), The natural iron fertilization exper-
763 iment KEOPS (KErguelen Ocean and Plateau compared Study): An overview,
764 *Deep Sea Research Part II: Topical Studies in Oceanography*, 55 (5–7), 559–565,
765 doi:10.1016/j.dsr2.2008.01.002.
- 766
- 767 Blanke, B., and S. Raynaud (1997), Kinematics of the Pacific Equatorial Undercurrent:
768 An Eulerian and Lagrangian approach from GCM results, *Journal of Physical Oceanog-*
769 *raphy*, 27 (6), 1038–1053, doi:10.1175/1520–0485.
- 770

771 Blanke, B., M. Arhan, G. Madec, and S. Roche (1999), Warm water paths in the
772 equatorial Atlantic as diagnosed with a general circulation model, *Journal of Physical*
773 *Oceanography*, *29*, 2753-2768.

774

775 Borriane, I., and R. Schlitzer (2013), Distribution and recurrence of phytoplankton
776 blooms around South Georgia, Southern Ocean, *Biogeosciences*, *10* (1), 217-231,
777 doi:10.5194/bg-10-217-2013.

778

779 Bowie, A. R., et al. (2015), Iron budgets for three distinct biogeochemical sites around
780 the Kerguelen Archipelago (Southern Ocean) during the natural fertilization study,
781 KEOPS-2, *Biogeosciences*, *12* (14), 4421-4445, doi:10.5194/bg-12-4421-2015.

782

783 Boyd, P. W., et al. (2000), A mesoscale phytoplankton bloom in the polar Southern Ocean
784 stimulated by iron fertilization, *Nature*, *407* (6805), 695-702, doi:10.1038/35037500.

785

786 Boyd, P. W. (2002), Environmental Factors Controlling Phytoplankton Processes in
787 the Southern Ocean, *Journal of Phycology*, *38* (5), 844-861, doi:10.1046/j.1529-
788 8817.2002.t01-1-01203.x.

789

790 Boyd, P. W. (2007), Biogeochemistry: iron findings, *Nature*, *446* (7139), 989-991,
791 doi:10.1038/446989a.

792

793 Boyd, P. W., et al. (2007), Mesoscale iron enrichment experiments 1993–2005: syn-
794 thesis and future directions, *Science*, *315* (5812), 612–617, doi:10.1126/science.1131669.

795

796 Boyd, P. W., and M. J. Ellwood (2010), The biogeochemical cycle of iron in the ocean,
797 *Nature Geoscience*, *3* (10), 675–682, doi:10.1038/ngeo964.

798

799 Boyd, P. W., K. R. Arrigo, R. Strzepek, and G. L. van Dijken (2012), Mapping phyto-
800 plankton iron utilization: Insights into Southern Ocean supply mechanisms, *Journal of*
801 *Geophysical Research: Oceans*, *117* (C6), C06009, doi:10.1029/2011JC007726.

802

803 Boyd, P. W., D. C. E. Bakker, and C. Chandler (2012), A New Database to Explore the
804 Findings from Large–Scale Ocean Iron Enrichments Experiments, *Oceanography*, *25*
805 (4), 64–71, doi: <http://dx.doi.org/10.5670/oceanog.2012.104>.

806

807 Boyer, T.P., J. I. Antonov, O. K. Baranova, C. Coleman, H. E. Garcia, A. Grodsky, D. R.
808 Johnson, R. A. Locarnini, A. V. Mishonov, T.D. O'Brien, C.R. Paver, J.R. Reagan, D.
809 Seidov, I. V. Smolyar, and M. M. Zweng, 2013: World Ocean Database 2013, NOAA
810 Atlas NESDIS 72, S. Levitus, Ed., A. Mishonov, Technical Ed.; Silver Spring, MD,
811 209, <http://doi.org/10.7289/V5NZ85MT>.

812

813 Brodeau, L., B. Barnier, A.–M.Treguier, T. Penduff, and S. Gulev (2010) An ERA40–
814 based 461 atmospheric forcing for global ocean circulation models. *Ocean Model.* *31*,
815 88–104.

816

817 Closset, I., M. Lasbleiz, K. Leblanc, B. Quguiner, A. J. Cavagna, M. Elskens, J. Navez,
818 and D. Cardinal (2014), Seasonal evolution of net and regenerated silica production
819 around a natural Fe-fertilized area in the Southern Ocean estimated with Si isotopic
820 approaches, *Biogeosciences*, *11* (20), 5827-5846, doi:10.5194/bg-11-5827-2014.

821

822 Comiso, J. C., C. R. McClain, C. W. Sullivan, J. P. Ryan, and C. L. Leonard (1993),
823 Coastal zone color scanner pigment concentrations in the Southern Ocean and rela-
824 tionships to geophysical surface features, *Journal of Geophysical Research*, *98* (C2),
825 2419, doi:10.1029/92jc02505.

826

827 de Baar, H. J., J. de Jong, T. M., D. C. Bakker, B. M. Loscher, C. Veth, U. Bath-
828 mann, and V. Smetacek (1995), Importance of iron for plankton blooms and carbon
829 dioxide drawdown in the Southern Ocean, *Nature*, *373*, 412 – 415, doi:10.1038/373412a0.

830

831 de Baar, H. J. W., L. J. A. Gerringa, P. Laan, and K. R. Timmermans (2008), Efficiency
832 of carbon removal per added iron in ocean iron fertilization, *Marine Ecology Progress*
833 *Series*, *364*, 269–282, doi:10.3354/meps07548.

834

835 d’Ovidio, F., A. Della Penna, T. W. Trull, F. Nencioli, M. I. Pujol, M. H. Rio, Y. H.
836 Park, C. Cott, M. Zhou, and S. Blain (2015), The biogeochemical structuring role
837 of horizontal stirring: Lagrangian perspectives on iron delivery downstream of the
838 Kerguelen Plateau, *Biogeosciences*, *12* (19), 5567-5581, doi:10.5194/bg-12-5567-2015.

839

840 Gille, S. T., M. M. Carranza, and R. Cambra (2014), Wind-induced upwelling in the
841 Kerguelen Plateau region, *Biogeosciences*, *11* (22), 6389-6400, doi:10.5194/bg-11-6389-
842 2014.

843

844 Graham, R. M., A. M. De Boer, E. van Sebille, K. E. Kohfeld, and C. Schlosser (2015),
845 Inferring source regions and supply mechanisms of iron in the Southern Ocean from
846 satellite chlorophyll data, *Deep Sea Research Part I: Oceanographic Research Papers*,
847 *104*, 9-25, doi:10.1016/j.dsr.2015.05.007.

848

849 Hewes, C. D., C. S. Reiss, M. Kahru, B. G. Mitchell, and O. Holm-Hansen (2008), Control
850 of phytoplankton biomass by dilution and mixed layer depth in the western Weddell-
851 Scotia Confluence, *Marine Ecology Progress Series*, *366*, 15-29, doi:10.3354/meps07515.

852

853 Holm-Hansen, O., M. Kahru, and C. D. Hewes (2005), Deep chlorophyll a maxima
854 (DCMs) in pelagic Antarctic waters. II. Relation to bathymetric features and dissolved
855 iron concentrations, *Marine Ecology Progress Series*, *297*, 71-81.

856

857 Korb, R. E., M. J. Whitehouse, and P. Ward (2004), SeaWiFS in the southern
858 ocean: spatial and temporal variability in phytoplankton biomass around South
859 Georgia, *Deep Sea Research Part II: Topical Studies in Oceanography*, *51*, 99-116,
860 doi:http://dx.doi.org/10.1016/j.dsr2.2003.04.002.

861

862 Korb, R. E., and M. Whitehouse (2004), Contrasting primary production regimes around
863 South Georgia, Southern Ocean: large blooms versus high nutrient, low chlorophyll
864 waters, *Deep Sea Research Part I: Oceanographic Research Papers*, 51 (5), 721–738,
865 doi:10.1016/j.dsr.2004.02.006.

866

867 Korb, R. E., M. J. Whitehouse, A. Atkinson, and S. E. Thorpe (2008), Magnitude and
868 maintenance of the phytoplankton bloom at South Georgia: a naturally iron-replete
869 environment, *Marine Ecology Progress Series*, 368, 75–91, doi:10.3354/meps07525.

870

871 Lasbleiz, M., K. Leblanc, S. Blain, J. Ras, V. Cornet–Barthaux, S. Hlias Nunige, and
872 B. Quguiner (2014), Pigments, elemental composition (C, N, P, and Si), and stoi-
873 chiometry of particulate matter in the naturally iron fertilized region of Kerguelen in
874 the Southern Ocean, *Biogeosciences*, 11 (20), 5931–5955, doi:10.5194/bg–11–5931–2014.

875

876 Le Bars, D., J. V. Durgadoo, H. A. Dijkstra, A. Biastoch, and W. P. M. De Ruijter
877 (2014), An observed 20–year time series of Agulhas leakage, *Ocean Science*, 10 (4),
878 601–609, doi:10.5194/os–10–601–2014.

879

880 Madec, G., (2008), NEMO reference manual, ocean dynamic component: NEMO–OPA,
881 Notes du pole de modelisation, Tech. Rep. 27, Institut Pierre Simmon Laplace (IPSL),
882 Paris, France.

883

884 Martin, J. H., R. M. Gordon, and S. E. Fitzwater (1990), Iron in Antarctic waters,
885 *Nature*, 345 (6271), 156–158, doi:10.1038/345156a0.

886

887 Martin, J. M. (1990), Glacial–interglacial CO₂ change: the iron hypothesis, *Paleoceanog-*
888 *raphy*, 5 (1), 1–13.

889

890 Marzocchi A., Hirschi J. J.–M., Holliday N.P., Cunningham S.A., Blaker A.T. and Coward
891 A.C. (2015) The North Atlantic subpolar circulation in an eddy–resolving global ocean
892 model, *Journal of Marine Systems*, 142, 126–143, doi:10.1016/j.jmarsys.2014.10.007.

893

894 Meijers, A. J. S., A. Klocker, N. L. Bindoff, G. D. Williams, and S. J. Marsland (2010),
895 The circulation and water masses of the Antarctic shelf and continental slope between
896 30 and 80degE, *Deep Sea Research Part II: Topical Studies in Oceanography*, 57 (9–10),
897 723–737, doi:10.1016/j.dsr2.2009.04.019.

898

899 Meredith, M. P., J. L. Watkins, E. J. Murphy, N. J. Cunningham, A. G. Wood, R. Korb,
900 M. J. Whitehouse, S. E. Thorpe, and F. Vivier (2003), An anticyclonic circulation
901 above the Northwest Georgia Rise, Southern Ocean, *Geophysical Research Letters*, 30
902 (20), doi:10.1029/2003gl018039.

903

904 Mongin, M., E. Molina, and T. W. Trull (2008), Seasonality and scale of the Kerguelen
905 plateau phytoplankton bloom: A remote sensing and modeling analysis of the influence
906 of natural iron fertilization in the Southern Ocean, *Deep Sea Research Part II: Topical*

907 *Studies in Oceanography*, 55 (5–7), 880–892, doi:10.1016/j.dsr2.2007.12.039.

908

909 Mongin, M. M., E. R. Abraham, and T. W. Trull (2009), Winter advection of iron
910 can explain the summer phytoplankton bloom that extends 1000 km downstream of
911 the Kerguelen Plateau in the Southern Ocean, *Journal of Marine Research*, 67, 225–237.

912

913 Moore, J. K., M. R. Abbott, and J. G. Richman (1999), Location and dynamics of
914 the Antarctic Polar Front from satellite sea surface temperature data, *Journal of*
915 *Geophysical Research*, 104 (C2), 3059, doi:10.1029/1998jc900032.

916

917 Moore, J. K., and M. R. Abbott (2000), Phytoplankton chlorophyll distributions and
918 primary production in the Southern Ocean, *Journal of Geophysical Research*, 105
919 (C12), 28709, doi:10.1029/1999jc000043.

920

921 Moore, C. M., S. Seeyave, A. E. Hickman, J. T. Allen, M. I. Lucas, H. Planquette,
922 R. T. Pollard, and A. J. Poulton (2007), Iron–light interactions during the CROZet
923 natural iron bloom and EXport experiment (CROZEX) I: Phytoplankton growth and
924 photophysiology, *Deep Sea Research Part II: Topical Studies in Oceanography*, 54
925 (18–20), 2045–2065, doi:10.1016/j.dsr2.2007.06.011.

926

927 Mosseri, J., B. Quiguiner, L. Armand, and V. Cornet–Barthaux (2008), Impact of iron
928 on silicon utilization by diatoms in the Southern Ocean: A case study of Si/N cycle
929 decoupling in a naturally iron–enriched area, *Deep Sea Research Part II: Topical*

930 *Studies in Oceanography*, 55 (5–7), 801–819, doi:10.1016/j.dsr2.2007.12.003.

931

932 Murphy, E. J., et al. (2013), Comparison of the structure and function of Southern Ocean
933 regional ecosystems: The Antarctic Peninsula and South Georgia, *Journal of Marine*
934 *Systems*, 109–110, 22–42, doi:10.1016/j.jmarsys.2012.03.011.

935

936 Orsi, A. H., T. Whitworth III, and W. D. Nowlin Jr (1995), On the meridional extent
937 and fronts of the Antarctic Circumpolar Current, *Deep Sea Research I*, 42 (5), 641–673.

938

939 Park, Y.-H., J.-L. Fuda, I. Durand, and A. C. Naveira Garabato (2008), Internal tides
940 and vertical mixing over the Kerguelen Plateau, *Deep Sea Research Part II: Topical*
941 *Studies in Oceanography*, 55 (5–7), 582–593, doi:10.1016/j.dsr2.2007.12.027.

942

943 Park, Y.-H., F. Roquet, I. Durand, and J.-L. Fuda (2008), Large-scale circulation over
944 and around the Northern Kerguelen Plateau, *Deep Sea Research Part II: Topical*
945 *Studies in Oceanography*, 55 (5–7), 566–581, doi:10.1016/j.dsr2.2007.12.030.

946

947 Park, Y.-H., I. Durand, E. Kestenare, G. Rougier, M. Zhou, F. d’Ovidio, C. Cott,
948 and J.-H. Lee (2014), Polar Front around the Kerguelen Islands: An up-to-date
949 determination and associated circulation of surface/subsurface waters, *Journal of*
950 *Geophysical Research: Oceans*, 119, doi:10.1002/2014jc010061.

951

952 Planquette, H., et al. (2007), Dissolved iron in the vicinity of the Crozet Islands, Southern
953 Ocean, *Deep Sea Research II*, 54, 1999 – 2019, doi:10.1016/j.dsr2.2007.06.019.

954
955 Pollard, R., R. Sanders, M. Lucas, and P. Statham (2007), The Crozet Natural Iron
956 Bloom and Export Experiment (CROZEX), *Deep Sea Research Part II: Topical Studies*
957 *in Oceanography*, 54 (18–20), 1905–1914, doi:10.1016/j.dsr2.2007.07.023.

958
959 Pollard, R. T., H. J. Venables, J. F. Read, and J. T. Allen (2007), Large-scale
960 circulation around the Crozet Plateau controls an annual phytoplankton bloom in
961 the Crozet Basin, *Deep Sea Research II*, 54, 1915 – 1929, doi:10.1016/j.dsr2.2007.06.012.

962
963 Pollard, R. T., et al. (2009), Southern Ocean deep-water carbon export enhanced by
964 natural iron fertilization, *Nature*, 457 (7229), 577-580, doi:10.1038/nature07716.

965
966 Popova, E. E., R. T. Pollard, M. I. Lucas, H. J. Venables, and T. R. Anderson
967 (2007), Real-time forecasting of ecosystem dynamics during the CROZEX experi-
968 ment and the roles of light, iron, silicate, and circulation, *Deep Sea Research Part II:*
969 *Topical Studies in Oceanography*, 54 (18-20), 1966-1988, doi:10.1016/j.dsr2.2007.06.018.

970
971 Popova, E. E., A. Yool, Y. Aksenov, and A. C. Coward (2013), Role of advection in
972 Arctic Ocean lower trophic dynamics: A modeling perspective, *Journal of Geophysical*
973 *Research*, 118, 1571–1586, doi:10.1002/jgrc.20126.

974

975 Poulton, A. J., C. Mark Moore, S. Seeyave, M. I. Lucas, S. Fielding, and P. Ward (2007),
976 Phytoplankton community composition around the Crozet Plateau, with emphasis on
977 diatoms and Phaeocystis, *Deep Sea Research Part II: Topical Studies in Oceanography*,
978 *54* (18-20), 2085-2105, doi:10.1016/j.dsr2.2007.06.005.

979
980 Read, J. F., R. T. Pollard, and J. T. Allen (2007), Sub-mesoscale structure and the
981 development of an eddy in the Subantarctic Front north of the Crozet Islands, *Deep-Sea*
982 *Research Part Ii-Topical Studies in Oceanography*, *54* (18-20), 1930-1948, doi:Doi
983 10.1016/J.Dsr2.2007.06.013.

984
985 Robinson, J., E. E. Popova, A. Yool, M. Srokosz, R. S. Lampitt, and J. R. Blundell
986 (2014), How deep is deep enough? Ocean iron fertilization and carbon seques-
987 tration in the Southern Ocean, *Geophysical Research Letters*, *41* (7), 2489-2495,
988 doi:10.1002/2013gl058799.

989
990 Sanial, V., P. van Beek, B. Lansard, F. d'Ovidio, E. Kestenare, M. Souhaut, M. Zhou,
991 and S. Blain (2014), Study of the phytoplankton plume dynamics off the Crozet Islands
992 (Southern Ocean): A geochemical-physical coupled approach, *Journal of Geophysical*
993 *Research-Oceans*, *119* (4), 2227-2237, doi:10.1002/2013jc009305.

994
995 Shaked, Y., and H. Lis (2012), Disassembling iron availability to phytoplankton, *Frontiers*
996 *in Microbiology*, *3* (123), doi:10.3389/fmicb.2012.00123.

997

- 998 Schallenberg, C., P. van der Merwe, F. Chever, J. T. Cullen, D. Lannuzel, and A. R.
999 Bowie (2015), Dissolved iron and iron(II) distributions beneath the pack ice in the
1000 East Antarctic (120E) during the winter/spring transition, *Deep Sea Research Part II:
1001 Topical Studies in Oceanography*, doi:10.1016/j.dsr2.2015.02.019.
- 1002
- 1003 Smetacek, V., P. Assmy, and J. Henjes (2004), The role of grazing in structuring
1004 Southern Ocean pelagic ecosystems and biogeochemical cycles, *Antarctic Science*, 16
1005 (4), 541-558, doi:10.1017/s0954102004002317.
- 1006
- 1007 Srokosz, M. A., J. Robinson, H. McGrain, E. E. Popova, and A. Yool (2015), Could the
1008 Madagascar bloom be fertilized by Madagascan iron?, *Journal of Geophysical Research:
1009 Oceans*, 120, doi:10.1002/2015JC011075.
- 1010
- 1011 Storm, T., M. Boettcher, M. Grant, M. Zuhlke, F. N., T. Jackson, and S. Sathyendranath
1012 (2013), Product User Guide, in *Ocean Colour Climate Change Initiative (OC_CCI) –
1013 Phase One*, edited by S. Groom, Plymouth Marine Laboratory, Plymouth, UK.
- 1014
- 1015 Tagliabue, A., J.-B. Salle, A. R. Bowie, M. Lvy, S. Swart, and P. W. Boyd (2014),
1016 Surface-water iron supplies in the Southern Ocean sustained by deep winter mixing,
1017 *Nature Geoscience*, 7 (4), 314-320, doi:10.1038/ngeo2101.
- 1018
- 1019 Takahashi, T., et al. (2009), Climatological mean and decadal change in surface
1020 ocean pCO₂, and net sea–air CO₂ flux over the global oceans, *Deep Sea Research Part*

- 1021 *II: Topical Studies in Oceanography*, 56 (8-10), 554-577, doi:10.1016/j.dsr2.2008.12.009.
- 1022
- 1023 Thomalla, S. J., N. Fauchereau, S. Swart, and P. M. S. Monteiro (2011), Regional
1024 scale characteristics of the seasonal cycle of chlorophyll in the Southern Ocean,
1025 *Biogeosciences*, 8 (10), 2849–2866, doi:10.5194/bg-8-2849-2011.
- 1026
- 1027 Tripathy, S. C., S. Pavithran, P. Sabu, H. U. K. Pillai, D. R. G. Dessai, and N. Anilkumar
1028 (2015), Deep chlorophyll maximum and primary productivity in Indian Ocean sector
1029 of the Southern Ocean: Case study in the Subtropical and Polar Front during austral
1030 summer 2011, *Deep Sea Research Part II: Topical Studies in Oceanography*, 118,
1031 240-249, doi:10.1016/j.dsr2.2015.01.004.
- 1032
- 1033 Tyrrell, T., A. Merico, J. J. Waniek, C. S. Wong, N. Metzl, and F. Whitney (2005),
1034 Effect of seafloor depth on phytoplankton blooms in high-nitrate, low-chlorophyll
1035 (HNLC) regions, *Journal of Geophysical Research*, 110 (G2), doi:10.1029/2005jg000041.
- 1036
- 1037 van Beek, P., M. Bourquin, J. L. Reyss, M. Souhaut, M. A. Charette, and C. Jeandel
1038 (2008), Radium isotopes to investigate the water mass pathways on the Kerguelen
1039 Plateau (Southern Ocean), *Deep Sea Research Part II: Topical Studies in Oceanogra-*
1040 *phy*, 55 (5–7), 622–637, doi:10.1016/j.dsr2.2007.12.025.
- 1041
- 1042 van der Merwe, P., et al. (2015), Sourcing the iron in the naturally fertilised bloom
1043 around the Kerguelen Plateau: particulate trace metal dynamics, *Biogeosciences*, 12

1044 (3), 739-755, doi:10.5194/bg-12-739-2015.

1045

1046 Venables, H. J., R. T. Pollard, and E. E. Popova (2007), Physical conditions controlling
1047 the development of a regular phytoplankton bloom north of the Crozet Plateau,
1048 Southern Ocean, *Deep Sea Research II*, 54, 1949 – 1965, doi:10.1016/j.dsr2.2007.06.014.

1049

1050 Venables, H., and C. M. Moore (2010), Phytoplankton and light limitation in the
1051 Southern Ocean: Learning from high–nutrient, high–chlorophyll areas, *Journal of*
1052 *Geophysical Research*, 115 (C2), doi:10.1029/2009jc005361.

1053

1054 Wadley, M. R., T. D. Jickells, and K. J. Heywood (2014), The role of iron sources and
1055 transport for Southern Ocean productivity, *Deep Sea Research Part I: Oceanographic*
1056 *Research Papers*, doi:10.1016/j.dsr.2014.02.003.

1057

1058 Ward, P., M. Whitehouse, R. Shreeve, S. Thorpe, A. Atkinson, R. Korb, D. Pond, and
1059 E. Young (2007), Plankton community structure south and west of South Georgia
1060 (Southern Ocean): Links with production and physical forcing, *Deep Sea Research I*,
1061 54, 1871–1889, doi:10.1016/j.dsr.2007.08.008.

1062

1063 Young, E. F., M. P. Meredith, E. J. Murphy, and G. R. Carvalho (2011), High–resolution
1064 modelling of the shelf and open ocean adjacent to South Georgia, Southern Ocean,
1065 *Deep Sea Research II*, 58, 1540–1552, doi:10.1016/j.dsr2.2009.11.003.

1066

1067 Young, E. F., S. E. Thorpe, N. Banglawala, and E. J. Murphy (2014), Variability
1068 in transport pathways on and around the South Georgia shelf, Southern Ocean:
1069 Implications for recruitment and retention, *Journal of Geophysical Research*, *119*,
1070 241–252, doi:10.1002/2013JC009348.

1071

1072 Zhang, Y., F. Lacan, and C. Jeandel (2008), Dissolved rare earth elements tracing
1073 lithogenic inputs over the Kerguelen Plateau (Southern Ocean), *Deep Sea Research Part*
1074 *II: Topical Studies in Oceanography*, *55* (5–7), 638–652, doi:10.1016/j.dsr2.2007.12.029.

1075

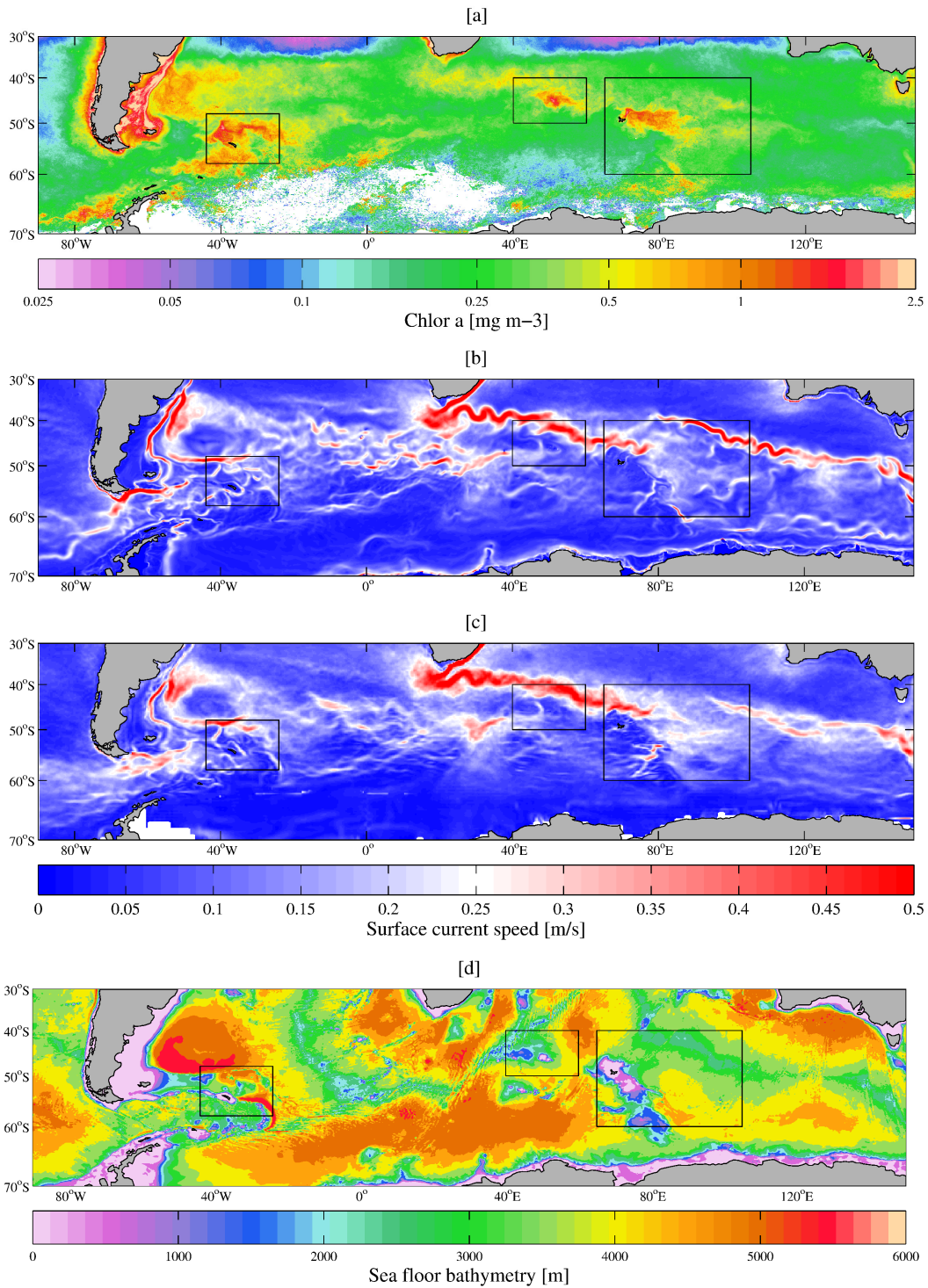


Figure 1. A Southern Ocean overview of satellite ocean color, satellite and modeled surface current speed, and the bathymetry in the model. Panel [a] is a decadal average, 1998 – 2007, of the chlorophyll-a concentration [mg m^{-3}] in the month of November. Panels [b] and [c] are the decadal averages (1998 – 2007) of surface current speed [$\text{m}^{-\text{s}}$], from the NEMO model, at $1/12^\circ$, and the Aviso data, at $1/4^\circ$ resolution, respectively. Panel [d] is the Southern Ocean bathymetry D R A F T within the NEMO $1/12^\circ$ model, contours are in meters below the sea surface. Black boxes denote the study areas: South Georgia left, Crozet islands middle, Kerguelen right.

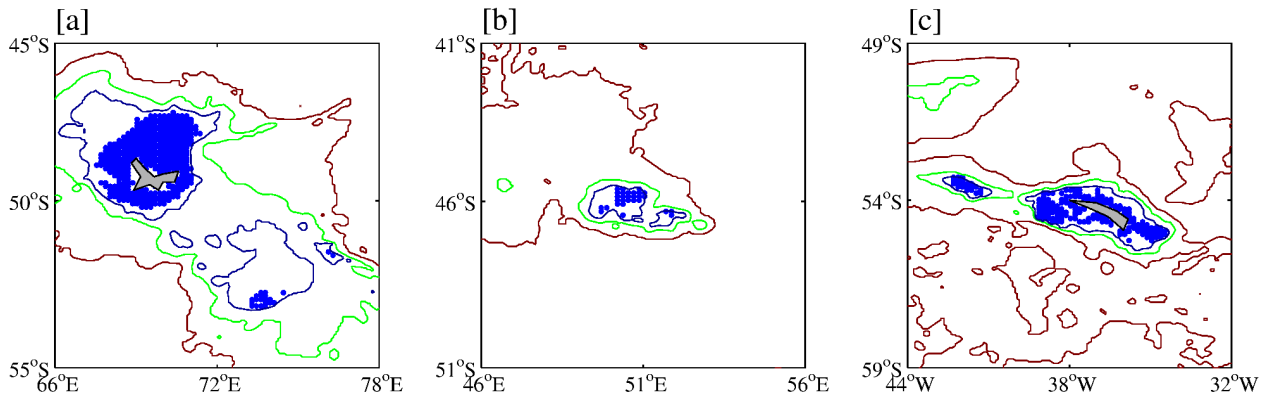


Figure 2. The starting positions of the Lagrangian particles around the islands. Particles are placed over shallow bathymetry (< 180 m), around Kerguelen and Heard Island, Crozet Islands, and South Georgia and Shag Rocks; plots [a], [b], and [c] respectively. In plots [a] and [c], only every other particle is plotted for clarity. The plot also includes contours of 500 m (dark blue), 1500 m (green) and 3000 m (red) isobaths. Note that the axis for each panel are not consistent.

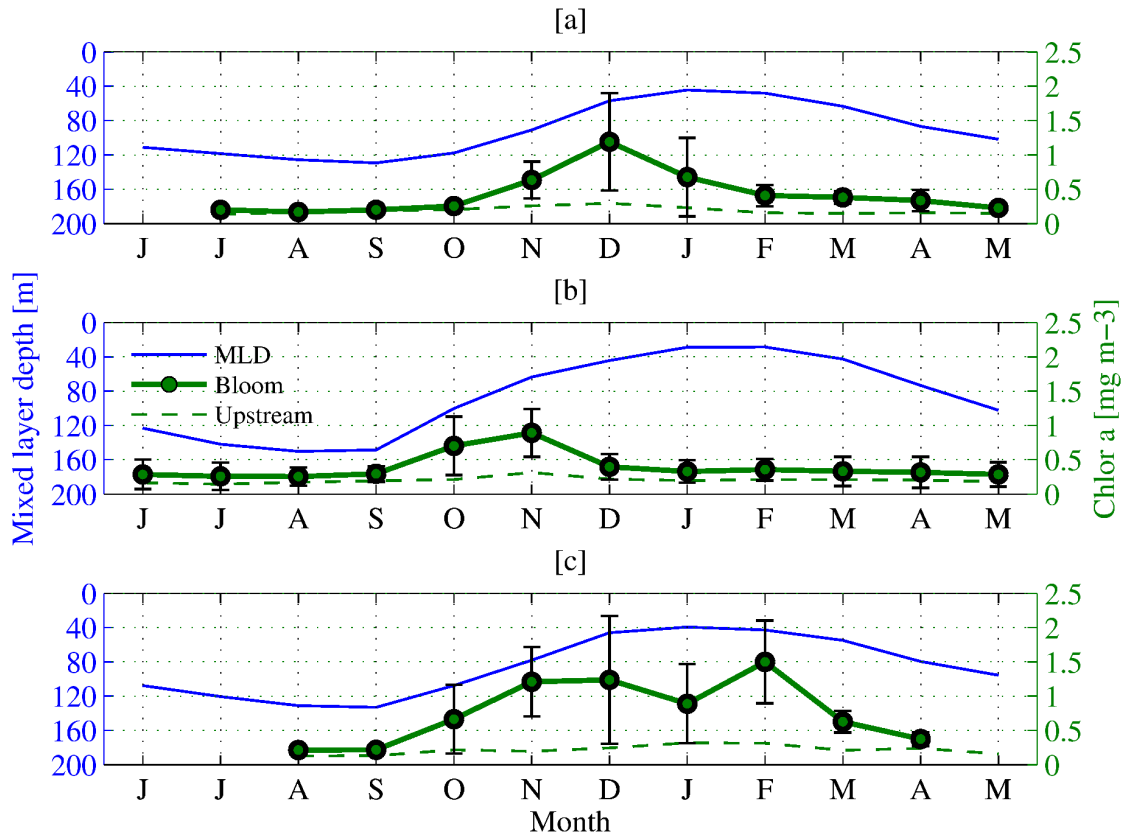


Figure 3. The average chlorophyll-a concentration [mg m^{-3}] (satellite ocean color) of each month over the 10 year period. Concentrations are from two locations, one inside (thick green line with markers) and one outside of the bloom region (dashed green line), for each island. The data points from inside the bloom region include error bars which are plus and minus one standard deviation in chlorophyll-a for each month, over the ten year period. The blue line represents the decadal average of the mixed layer depth of each location inside the bloom. Panels [a], [b], and [c] are Kerguelen, Crozet and South Georgia. Note the x axis, ‘Month’, begins from June through to May.

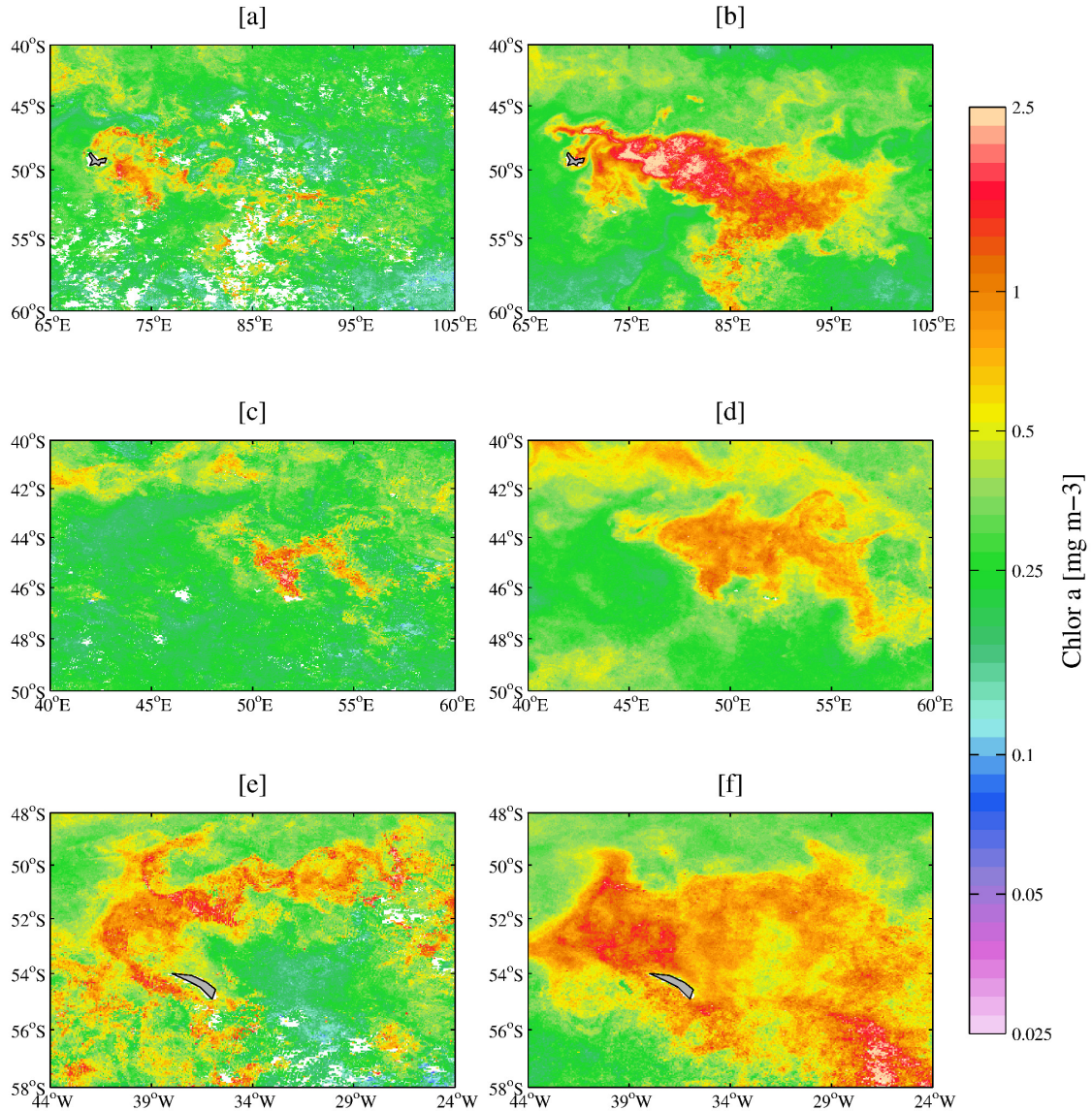


Figure 4. Example years of satellite ocean color plots of each island. Chlorophyll-a concentrations have been averaged over the bloom period for each year. The top row is Kerguelen (bloom period: Nov – Jan), years 2000 ([a]) and 2003 ([b]); the middle row is Crozet (bloom period: Oct – Dec), years 2001 ([c]) and 2004 ([d]); and the bottom row is South Georgia (bloom period: Oct – Apr), years 2006 ([e]) and 2002 ([f]). Panels [a], [c], and [e] are examples of a small bloom extent during the 1998 – 2007 year period, and panels [b], [d], and [f] are years with a large bloom extent.

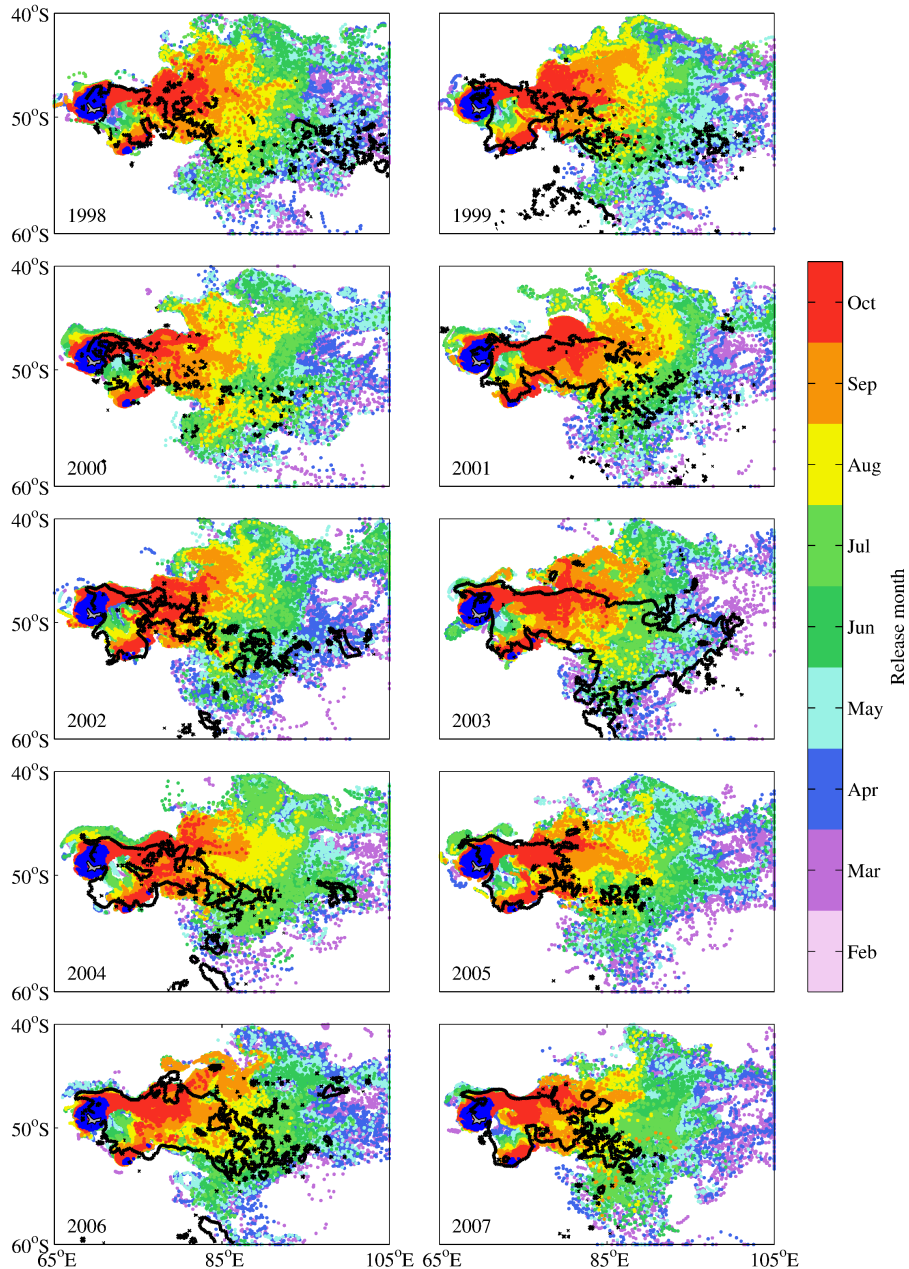


Figure 5. Extent of Lagrangian trajectories around Kerguelen. 8240 particles were released monthly from their starting positions, denoted in blue, however only every second particle is shown here for clarity. Particle trajectories in October (preceding the start of the bloom), are shown here for clarity. Particle trajectories in October (preceding the start of the bloom), are depicted by colored markers. The color of the trajectory relates to the month in which it was released as indicated by the color bar. The black contour represents the averaged bloom area, over November – January, of chlorophyll-*a* concentrations above 0.5 mg m^{-3} . Only trajectories that are shallower than 200m are included in this plot.

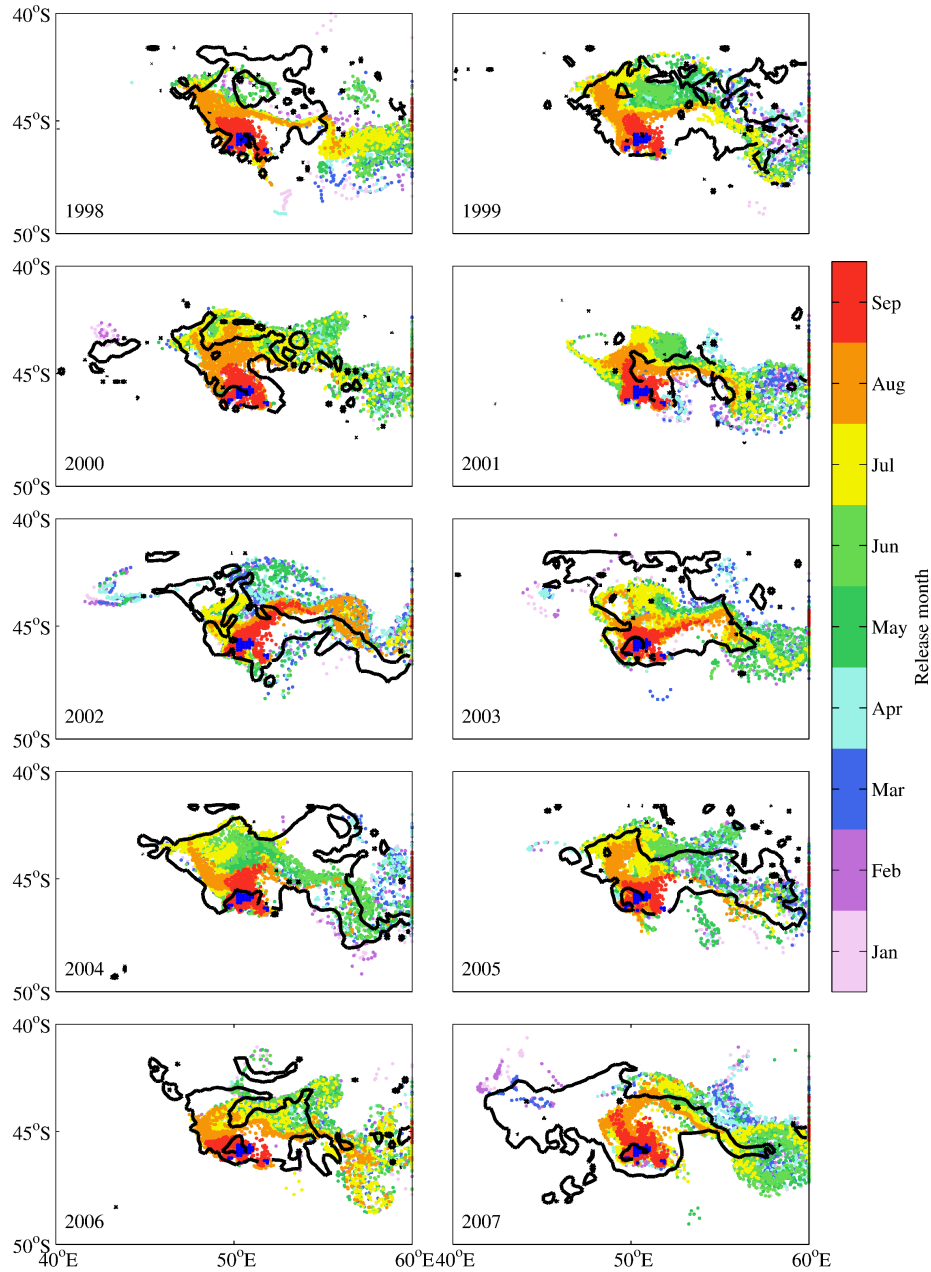


Figure 6. Extent of Lagrangian trajectories around Crozet. 465 particles were released monthly from their sing positions, denoted in blue, however only every second particle is shown here for clarity. Trajectories in September (preceding the start of the bloom), are depicted by colored markers. The color of the trajectory relates to the month in which it was released as indicated by the color bar. The black contour represents the averaged bloom area, over October – December, of chlorophyll-a concentrations above 0.5 mg m^{-3} . Only trajectories that are shallower than 200m are included in this plot.

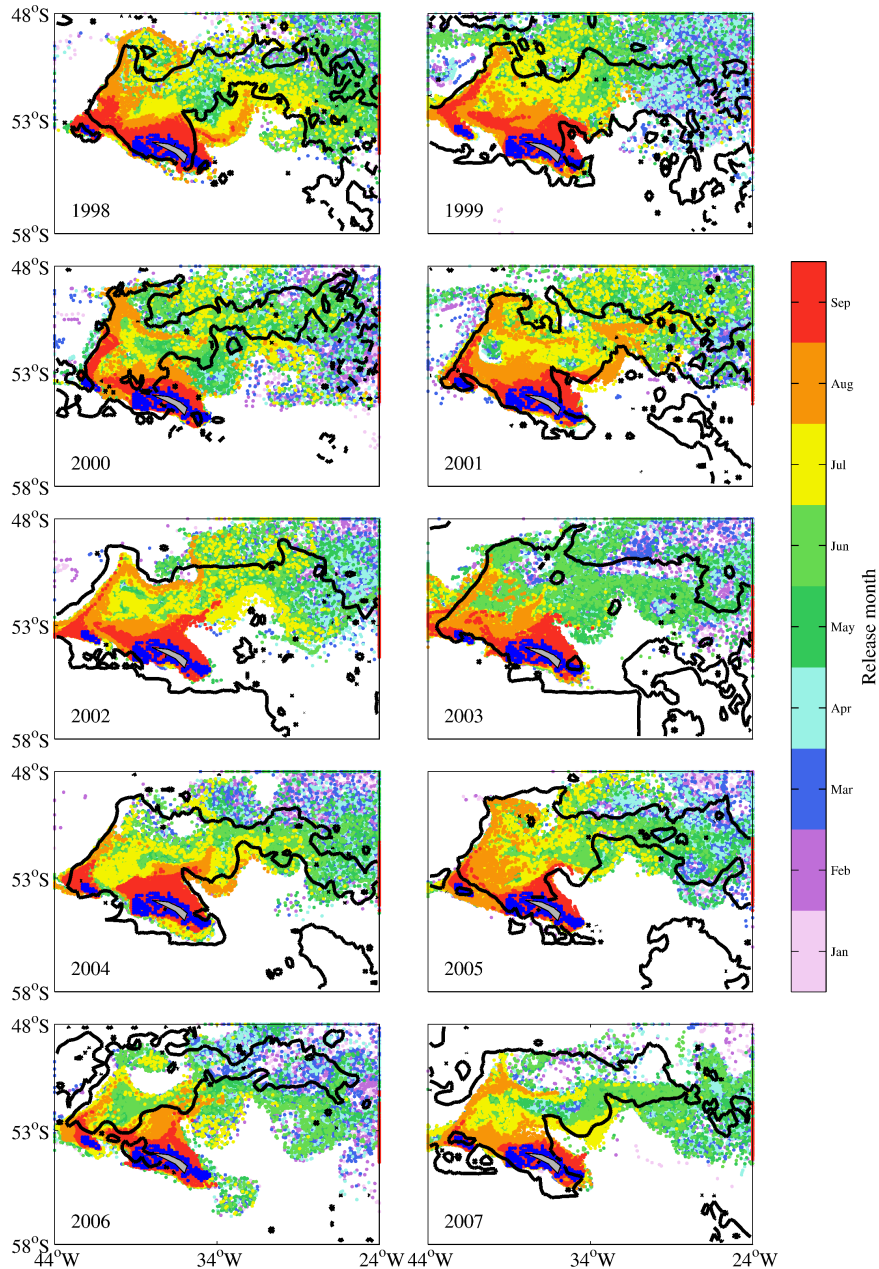


Figure 7. Extent of Lagrangian trajectories around South Georgia. 2820 particles were released monthly from their starting positions, denoted in blue, however only every second particle is shown here for clarity. Trajectories, in October (preceding the start of the bloom), are depicted by colored markers. The color of the trajectory relates to the month in which it was released as indicated by the colorbar. The black contour represents the averaged bloom area, over October – April, of chlorophyll-*a* concentrations above 0.5 mg m^{-3} . Only trajectories that are shallower than 200m are included in this plot.

Table 1. Size of the annual bloom and fertilized patch around Kerguelen, and the percent of each area that is overlapped by the other. ^a

Year	Bloom Area (km ²)	Fertilized patch (km ²)	Bloom Overlap (%)	Fertilized Overlap (%)
1998	674572	2731476	74	18
1999	803847	2676533	64	19
2000	339783	2693883	78	10
2001	832765	2593000	84	27
2002	613450	2621786	75	18
2003	1602173	2435464	73	48
2004	729515	2637034	72	20
2005	532218	2568354	84	17
2006	1056154	2539699	82	34
2007	640068	2358635	86	23

^a Bloom Area is the total area of the average (November to January) chl-a concentration above 0.5 mg m⁻³; Fertilized patch is the extent of particle trajectories in October (prior to the start of the bloom); Bloom Overlap is the percent of the bloom area overlapped by the fertilized patch; Fertilized Overlap is the percent of the fertilized patch overlapped by the bloom

Table 2. Size of the annual bloom and fertilized patch around Crozet, and the percent of each area that is overlapped by the other. ^a

Year	Bloom Area (km ²)	Fertilized patch (km ²)	Bloom Overlap (%)	Fertilized Overlap (%)
1998	223784	216357	35	36
1999	300810	251913	52	62
2000	168707	259734	59	38
2001	70586	231342	60	18
2002	195589	238834	42	34
2003	299167	232525	41	52
2004	355097	252176	48	67
2005	258354	246721	54	56
2006	209982	244683	47	40
2007	342084	282999	32	39

^a Bloom Area is the total area of the average (October to December) chl-*a* concentration above 0.5 mg m⁻³; Fertilized patch is the extent of particle trajectories in September (prior to the start of the bloom); Bloom Overlap is the percent of the bloom area overlapped by the fertilized patch; Fertilized Overlap is the percent of the fertilized patch overlapped by the bloom

Table 3. Size of the annual bloom and fertilized patch around South Georgia, and the percent of each area that is overlapped by the other. ^a

Year	Bloom Area (km ²)	Fertilized patch (km ²)	Bloom Overlap (%)	Fertilized Overlap (%)
1998	527788	801679	79	52
1999	671337	864382	70	54
2000	453359	810443	79	44
2001	560929	798532	74	52
2002	946833	704231	50	67
2003	854692	750085	56	64
2004	587281	713427	69	57
2005	626285	700466	66	59
2006	414108	703676	56	33
2007	543833	573456	61	58

^a Bloom Area is the total area of the average (October to April) chl-*a* concentration above 0.5 mg m⁻³; Fertilized patch is the extent of particle trajectories in September (prior to the start of the bloom); Bloom Overlap is the percent of the bloom area overlapped by the fertilized patch; Fertilized Overlap is the percent of the fertilized patch overlapped by the bloom

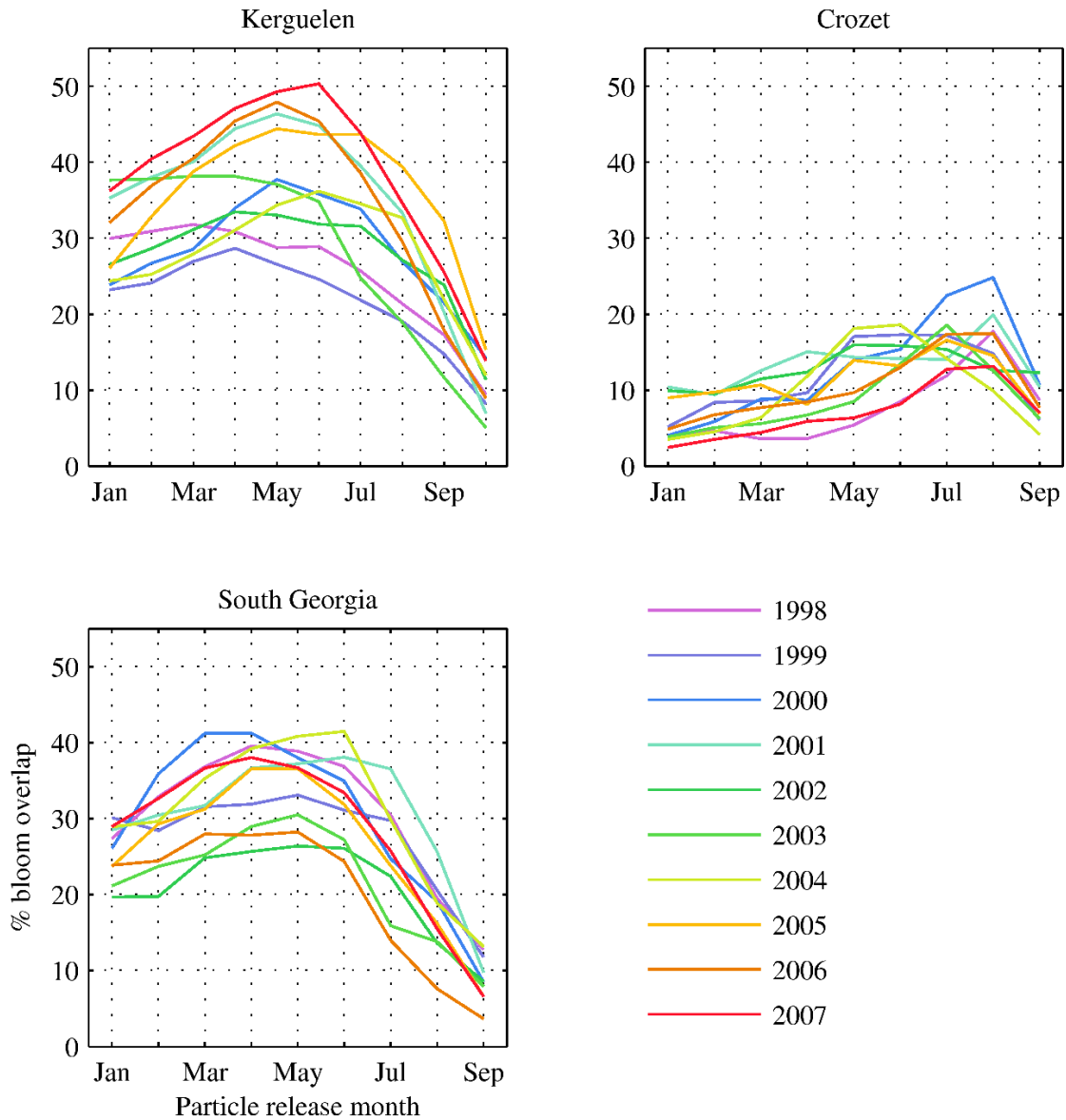


Figure 8. The percent of the bloom area overlapped by Lagrangian trajectories from each monthly release for each year. For each monthly release of particles, trajectories that were within the bloom area, in the month that is prior to the start of the bloom, were recorded and used to calculate the percentage area coverage of the bloom by Lagrangian trajectories. Any particles deeper than 200 m were not included. The y axis, *% bloom overlap*, indicates the percentage of the bloom area overlapped by particles from each monthly release shown on the x axis, *Particle release month*. Each colored line represents an individual year.

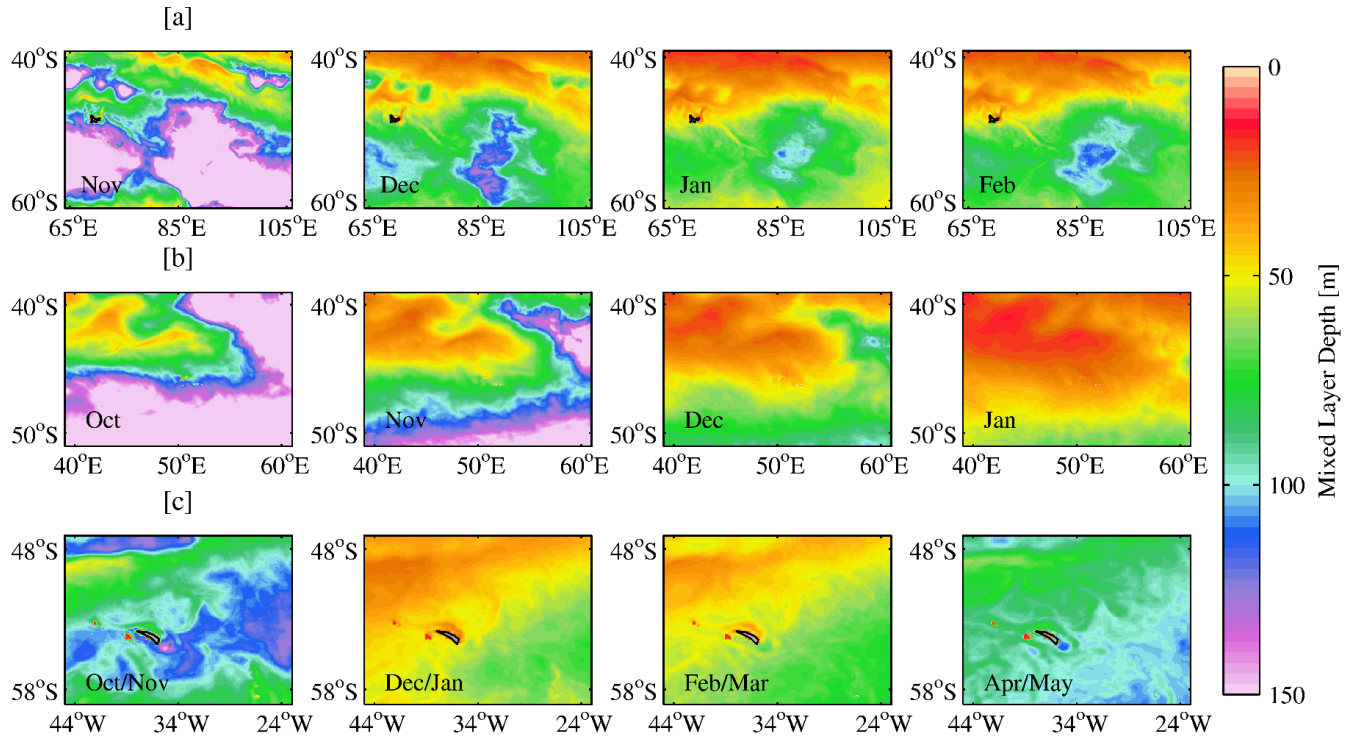


Figure 9. Monthly climatologies (decadal, 1998 – 2007) of the modeled mixed layer depth, calculated online by the NEMO model, around Kerguelen, Crozet and South Georgia. The color scale is m below the surface, with warm colors indicating shallow depths and cold colors representing deeper depths.

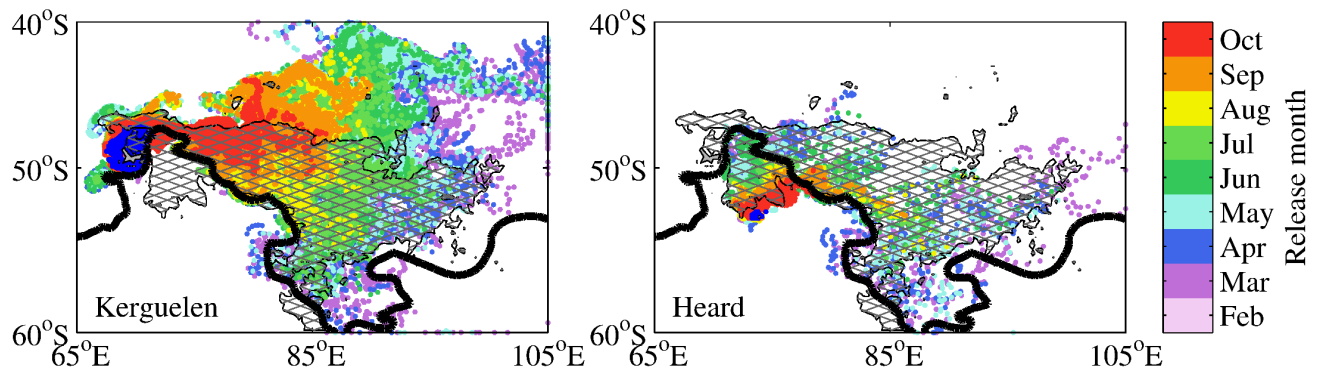


Figure 10. Lagrangian trajectories originating from the Kerguelen and Heard Islands in 2003. Collectively, 8240 particles were released monthly from their starting positions, denoted in blue, however only every second particle is shown here for clarity. Particle trajectories are depicted by colored markers, with the color of the marker relating to the month in which it was released as indicated by the color bar. Gray hatching represents the bloom area, averaged over November – January, where chlorophyll-*a* concentrations are above 0.5 mg m^{-3} . The thick black contour represents the approximate location of the Polar Front in the model for 2003. Only trajectories that are shallower than 200m are included in this plot.